LES HOUCHES, ECOLE D'ÉTÉ DE PHYSIQUE THÉORIQUE

Session		
I	1951	Mécanique quantique. Théorie quantique des champs
II	1952	Quantum mechanics. Mécanique statistique. Chapitres de physique nucléaire
III	1953	Quantum mechanics. Etat solide. Mécanique statistique. Elementary particles
IV	1954	Mécanique quantique. Théorie des collisions; two-nucleon interaction. Electrodynamique quantique
V	1955	Quantum mechanics. Non-equilibrium phenomena. Réactions nucléaires. Interaction of a nucleus with atomic and molecular fields
VI	1956	Quantum perturbation theory. Low temperature physics. Quantum theory of solids; dislocations and plastic properties. Magnetism; ferromagnetism
VII	1957	Théorie de la diffusion; recent developments in field theory. Interaction nucléaire; interactions fortes. Electrons de haute énergie. Experiments in high energy nuclear physics
VIII	1958	Le problème à *N* corps (Dunod, Wiley, Methuen)
IX	1959	La théorie des gaz neutres et ionisés (Hermann, Wiley)
X	1960	Relations de dispersion et particules élémentaires (Hermann, Wiley)
XI	1961	La physique des basses températures. Low temperature physics (Gordon and Breach, Presses Universitaires)
XII	1962	Géophysique extérieure. Geophysics: the earth's environment (Gordon and Breach)
XIII	1963	Relativité, groupes et topologie. Relativity, groups and topology (Gordon and Breach)
XIV	1964	Optique et électronique quantiques. Quantum optics and electronics (Gordon and Breach)
XV	1965	Physique des hautes énergies. High energy physics (Gordon and Breach)
XVI	1966	Hautes énergies en astrophysique. High energy astrophysics (Gordon and Breach)
XVII	1967	Problème à *N* corps. Many-body physics (Gordon and Breach)
XVIII	1968	Physique nucléaire. Nuclear physics (Gordon and Breach)
XIX	1969	Aspects physiques de quelques problèmes biologiques. Physical problems in biology (Gordon and Breach)
XX	1970	Mécanique statistique et théorie quantique des champs. Statistical mechanics and quantum field theory (Gordon and Breach)
XXI	1971	Physique des particules. Particle physics (Gordon and Breach)
XXII	1972	Physique des plasmas. Plasma physics (Gordon and Breach)
XXIII	1972	Les astres occlus. Black holes (Gordon and Breach)
XXIV	1973	Dynamique des fluides. Fluid dynamics (Gordon and Breach)
XXV	1973	Fluides moléculaires. Molecular fluids (Gordon and Breach)
XXVI	1974	Physique atomique et moléculaire et matière interstellaire. Atomic and molecular physics and the interstellar matter (North-Holland)
June Inst.	1975	Structural analysis of collision amplitudes (North-Holland)
XXVII	1975	Aux frontières de la spectroscopie laser. Frontiers in laser spectroscopy (North-Holland)
XXVIII	1975	Méthodes en théorie des champs. Methods in field theory (North-Holland)
XXIX	1976	Interactions électromagnétiques et faibles à haute énergie. Weak and electromagnetic interactions at high energy (North-Holland)
XXX	1977	Ions lourds et mésons en physique nucléaire. Nuclear physics with heavy ions and mesons (North-Holland)

En préparation		
XXXI	1978	La matière mal condensée. Ill-condensed matter
XXXII	1979	Cosmologie physique. Physical cosmology
XXXIII	1979	Biomembranes et communications intercellulaires. Biomembranes and intercellular communications

LES HOUCHES

SESSION XXX

4 Juillet – 20 Août 1977

IONS LOURDS ET MÉSONS EN PHYSIQUE NUCLÉAIRE

NUCLEAR PHYSICS WITH HEAVY IONS AND MESONS

VOLUME 1

Edité par

ROGER BALIAN, MANNQUE RHO, GEORGES RIPKA

Saclay

1978
NORTH-HOLLAND PUBLISHING COMPANY
AMSTERDAM · NEW YORK · OXFORD

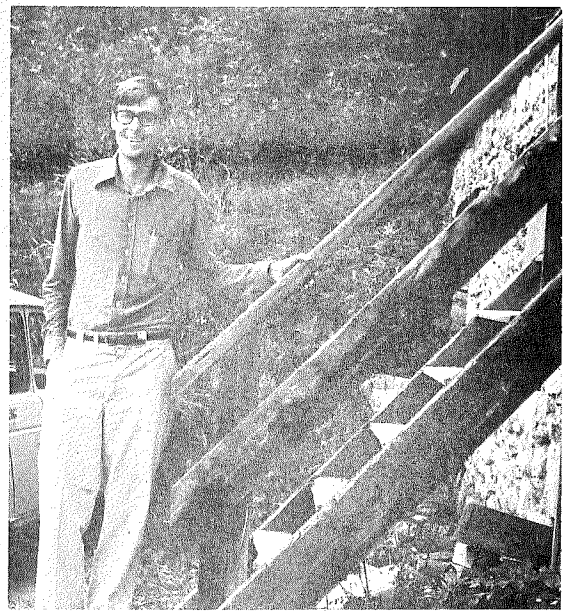

Contents

R. Balian et al., eds.
Les Houches, Session XXX, 1977. Ions lourds et mésons en physique nucléaire/ Nuclear physics with heavy ions and mesons

COURSE 3

DYNAMICS OF HEAVY ION COLLISIONS*

George F. BERTSCH

Physics Department, Cyclotron Laboratory, Michigan State University, East Lansing, Mich. 48824, USA

* Supported by the National Science Foundation.

1. Phenomena in heavy ion collisions

Collisions between complex nuclei were first studied in cosmic ray experiments in the late 1940's and in accelerator experiments in the early 1950's. Nevertheless, the subject is still largely unexplored. Both experimental techniques left a wide gap in accessible energy, a gap which is not completely closed even today. Particularly for the intermediate energy collisions, the questions that we need to ask are not questions of detail but questions of the very nature of the phenomena that occur. The theoretical task is to see how these phenomena can be comprehended and incorporated into our overall view of nuclei and many-body dynamics. In discussing the theory at this preliminary stage, it is important to keep in mind the limitations and possibilities of the experiments. We will begin with a short survey of what has been observed in heavy ion collisions.

The qualitative behavior of the collisions depends very much on the collision energy. At low energy, the nuclei behave like extended objects with a short-range attraction, i.e. like sticky balls. For short time intervals, these objects are fairly rigid, and for longer time intervals, they behave as liquids. At medium energies, the nuclei interpenetrate and become compressed during the course of a collision. At high energies, the nuclear binding becomes a small perturbation on the dynamics of the nucleons, and the reaction proceeds as independent collisions of the constituent particles.

There are two domains of energy experimentally accessible today for heavy ion collisions. The range of energy 0–8 MeV per nucleon is available in a number of laboratories. There is a gap in energies from about 10 MeV/A to 250 MeV/A. Energies in the range 250 MeV/A to 2 GeV/A are produced in the Berkeley Bevatron-Superhilac accelerators. The kinds of projectiles most commonly produced in these accelerators are the noble gases Ne, Ar, Kr, and Xe. The situation is better with α particles. The range of energies available for α projectiles is almost continuous from low energy to 2 GeV/A.

The energies in the low regime, up to 8 MeV/A bombarding energy, are quite small on the scale of nuclear energies. First, there is the Coulomb

barrier to be overcome in any collision. Secondly, for a collision of two identical ions the amount of energy available per particle in the combined system is $\frac{1}{4}$ the incident energy per particle: a factor of $\frac{1}{2}$ for the total energy in the center of mass, and another factor of $\frac{1}{2}$ for the greater number of nucleons in the combined system than in the projectile. The energy per particle available with present day accelerators in the low energy range is thus much smaller than the binding energy per nucleon. Furthermore, at these low energies the duration of a collision is longer than the transit time of a nucleon at the Fermi level. This implies that the whole nucleus responds coherently to the collision. In the high energy regime, the opposite is true. Nucleons are undergoing violent collisions with each other, and the binding energy is only a small perturbation on their motion.

Unfortunately, the experiments provide only indirect information on the dynamics of the collisions. Most experiments measure the abundances of the products of the reaction: kinds of particles, their energies and angular distributions. Most of these products are formed long after the reaction took place, so inferences about the reaction itself are indirect. An interesting exception to this statement is the production of pions, which will be discussed in sect. 6.

Because the data have so many variables, the experimentalists need some simplifying concepts merely to present the data. For low energy collisions, many classical concepts are available and have utility, for example the idea of a classical trajectory. In high energy collisions, so far only temperature has been used to organize the data.

1.1. Low energy collisions

The outcome of the collision depends of course on the impact parameter. Experimental data for collisions of water droplets [1.1] are shown in fig. 1. At low energies and small impact parameters, fusion takes place. At higher energies and larger impact parameters the final state has two or more drops in it. But note that this can happen also for head-on collisions. In fact the motion can be quite complicated, with the system breaking up as a chain of beads.

In nuclear collisions, the character of the reaction is thought to depend on the impact parameter also. The three main categories of reaction are fusion, strongly damped collisions, and quasielastic scattering, and their relative importance at different impact parameters is indicated in fig. 2. By quasi-elastic scattering is meant excitation that involves only a few MeV of energy loss, populating states near the ground state. This type of

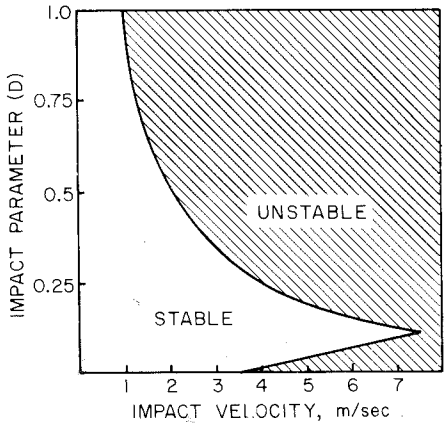

Fig. 1. Collisions of 300 μm water droplets, (ref. [1.1]).

reaction dominates at large impact parameter, where the Coulomb field or the edge of the nuclear field is responsible for the excitation. I expect that this type of reaction is discussed in detail in the lectures by Brink and by Schaeffer. One thing that has been learned is that the major features of such reactions are determined by the dynamics of two bodies interacting

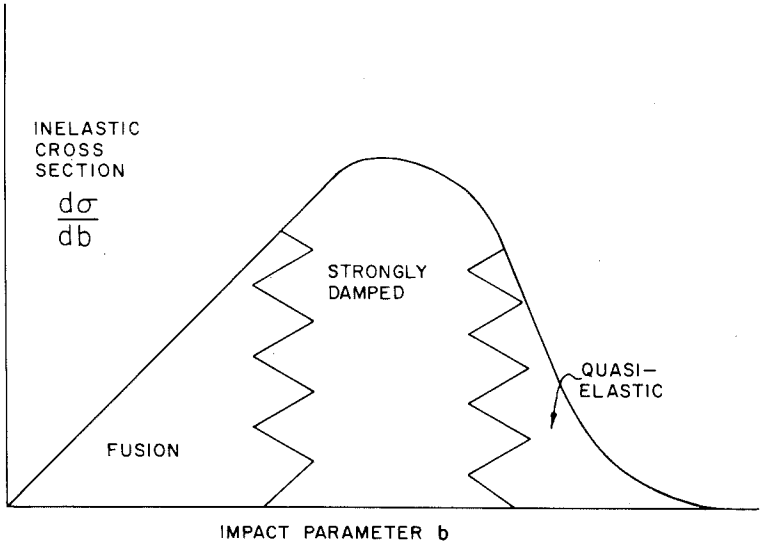

Fig. 2. Main categories of reaction cross-section as a function of impact parameter.

via the Coulomb plus nuclear potential. Such features include the broad peaks in angular distributions as well as the narrow wiggles, and correlations between the transfer of energy, angular momentum, and mass. The wealth of data on specific states allows the nuclear part of the interaction to be quite well determined in the far surface region. Elastic scattering determines the potential depth at the strong absorption radius [1.2]. This is defined as the radius of the classical turning point for a trajectory in which half the flux is absorbed. The slope of the potential is also fairly well determined at this point. A rough formula for the strong absorption radius, determined from elastic scattering, is [1.3]

$$R_{\mathrm{SA}} = 1.4(A_1^{1/3} + A_2^{1/3})\,. \tag{1.1}$$

The potential depth at this radius is of the order of 1 MeV, and the slope of the potential at this point is 1.5–2 MeV/fm. In most cases the excitation of low-lying states of colliding nuclei may be calculated by considering only the perturbative effect of the potential field of one nucleus on the other nucleus. This also includes the description of the transfer of one or two nucleons. In a few cases not understood at present this theory gives incorrect wiggles in the angular distributions.

The second major category of reaction, the strongly damped collisions, is characterized by a large energy loss while some of the features of a two-body reaction are preserved. An example of the energy distribution of the nuclei emerging from a heavy ion collision is shown in fig. 3, taken from ref. [1.4]. The sharp peak in this spectrum for small energy losses is the quasielastic scattering. There is also a broad peak for energy losses of 200–300 MeV, which contains the strongly damped collisions. This second peak is even more pronounced in the lighter ion reactions such as ^{40}Ar + ^{232}Th. The kinetic energy of the fragments in this second peak is entirely due to the Coulomb repulsion between the separating fragments. For example, in the case of $^{84}_{36}$Kr + $^{209}_{83}$Bi, the Coulomb energy of two touching spheres with a separation given by eq. (1.1) is

$$V = \frac{Z_1 Z_2 e^2}{R} = \frac{(36)(83)(1.44)}{(14.4)} = 299\ \mathrm{MeV}\,. \tag{1.2}$$

In the experiment, the initial energy in the center of mass is

$$E_{\mathrm{cm}} = \frac{209}{209 + 84} \times 712 = 499\ \mathrm{MeV}\,.$$

The energy loss, if the fragments separate with no kinetic energy and only the potential energy of eq. (1.2), would be 200 MeV. This is indicated by an arrow in the figure. In fact, even greater energy losses are observed. This

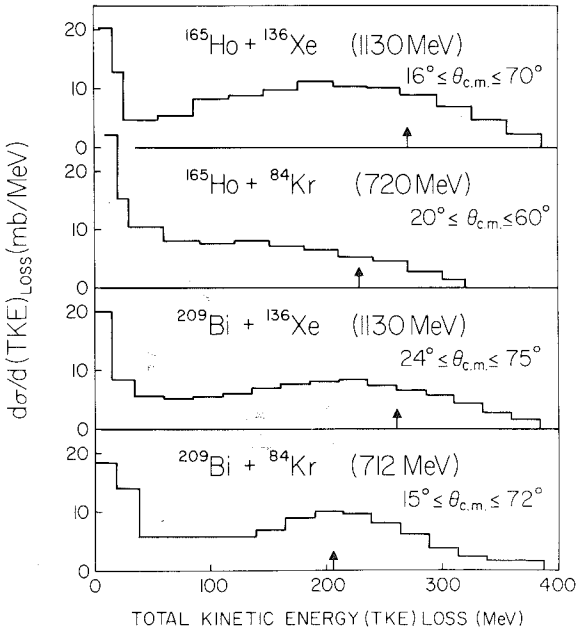

Fig. 3. Energy distribution of the nuclei emerging from a heavy ion collision. From ref. [1.4].

could indicate that the compound system greatly elongates before it splits, or it could indicate that small fragments carry off a great deal of energy.

Despite the large energy loss, the angular distribution of the strongly damped collisions looks like a direct reaction, which peaks at angles characteristic of the two-body dynamics. This is quite surprising, since the expectation is that if the kinetic energy loss were complete, the system would lose memory of angular orientation. The mass distribution of the outgoing fragments also shows preservation of the memory of initial conditions. There is a range of masses emerging from the strongly damped collision, but the most abundant masses are those close to the initial masses. Since the charge of the products can be measured, it is possible to study the distribution in θ or in E as a function of Z. A diffusion picture can be applied to the resulting curves: the more change there is in any of these variables from the elastic case, the more spread there is in the remaining variables. To describe the spreading of some function about a mean, a natural thought is to consider the theory of diffusion. However, this is beyond the scope of this chapter.

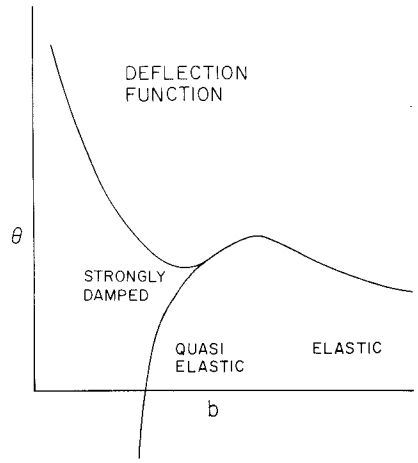

Fig. 4. The deflection function.

A theoretical construct which has proven useful in the discussion of the two categories of reaction discussed above is the deflection function. This is the classical deflection angle in a collision as a function of the impact parameter. This is sketched in fig. 4. For large impact parameters, the deflection function is positive because of the Coulomb scattering. Any region where it is flat means that a large amount of flux will go into a small angular range. The strongly damped collision data suggest that it is nearly flat for a range of impact parameters inside the impact parameter corresponding to the strong absorption radius. For light ions, at a small enough impact parameter the deflection function goes to $-\infty$, corresponding to capture and fusion of the two nuclei. Whether this happens in the heavier systems, or whether the deflection function goes to $+180°$ at zero impact parameter, is still not clear.

Fusion, the third main kind of reaction, is harder to study than the other reactions. Even the definition of fusion causes some problems, because the final state is sure to have more than one particle – there is roughly one evaporation neutron for each 8 MeV of excitation. Furthermore, if the charge of the fused system is above 90, it is likely to decay by fission. Limiting ourselves to the less highly charged systems, the recoiling fused system can be detected directly, but since the recoil energy is generally low, it is difficult to make accurate measurements. Special techniques have been used for fusion measurements, making use of special detectors sensitive only to high Z particles, or making use of radioactivity of the fusion

product [1.5]. It is also possible to use the standard counter technique of measuring E and dE/dx of the product [1.6, 1.7]. These measurements show that the dominant inelastic process for light nuclei is fusion. For projectiles up to Ar, the ratio of fusion to total reaction cross-section is in the range

$$\sigma_{CF}/\sigma_R \approx 0.6\text{–}0.8\,, \tag{1.3}$$

with the lower figure for energies higher than the Coulomb barrier. When the reaction is done with heavy nuclei, so that the charge of the combined system is greater than for the heaviest nuclei known, no evidence of fusion is seen. In the reactions Kr + Bi and Xe + Bi, the reaction cross-sections measured are consistent with being entirely of the strongly damped type.

There are two features of the fusion cross-section that can be measured quantitatively, namely the threshold energy and the rate at which the cross-section increases above threshold. A convenient parameterization is based on the model that fusion takes place if and only if the nuclei approach to within some critical radius R_B. If the threshold energy is V_B, then the fusion cross-section above threshold is

$$\sigma_F = \pi R_B^2(1 - V_B/E_{in})\,. \tag{1.4}$$

This formula fits the data on light nuclei fairly well [1.7]. A classical model can be constructed for the fusion process, in which it is assumed that the two nuclei interact through a potential consisting of the Coulomb field and a short-range nuclear attraction. In the model fusion takes place if the nuclei overcome the potential barrier. The barrier height is V_B, and the derivative of the potential vanishes at R_B. This can then be used to infer the nuclear interaction at the point R_B. An interesting question is whether this potential is consistent with the potential determined at the strong absorption radius. If the potential is parameterized by the function

$$V = V_0 \exp[-(r - R_0/a)]\,, \tag{1.5}$$

the potentials are found to agree to within a factor of two or so [1.7].

The further decay of the collision products provides information on the state of the products. The energy distribution of the fragments can often be parameterized in terms of a temperature. The concept of temperature implies that there is a statistical equilibrium in the competition among decays. If this is valid, the emission of low-energy (evaporation) neutrons is given by the spectrum

$$d\sigma/dE \sim E \exp(-E/T)\,, \tag{1.6}$$

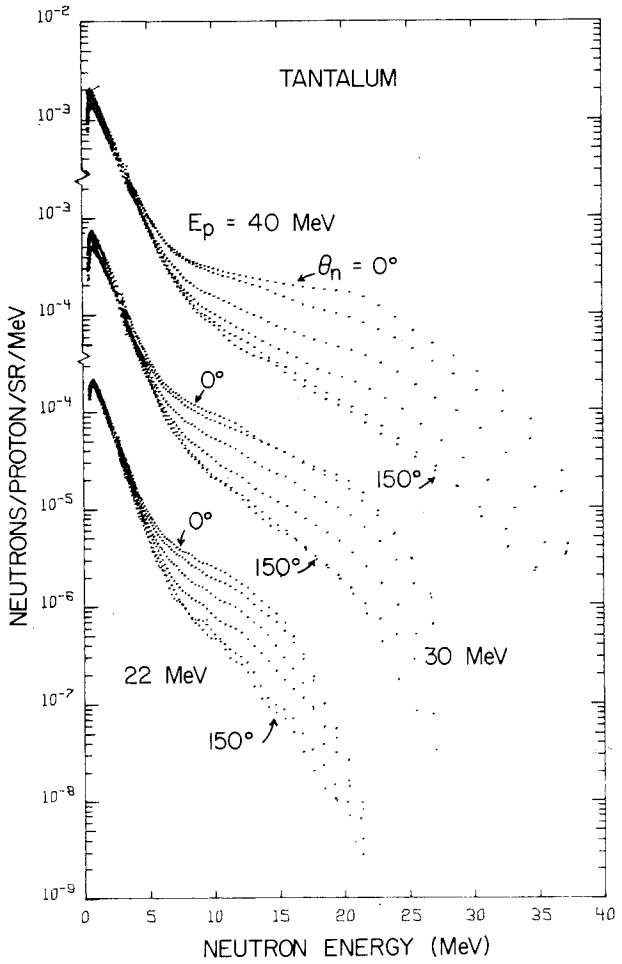

Fig. 5. Neutron spectra from proton-induced reactions on Ta (ref. [1.22]).

where T is the temperature in MeV. An example of a neutron spectrum is given in fig. 5 for the proton bombardment of Ta [1.22]. It may be seen that up to 5 MeV the distribution is exponential; from the graph may be inferred a temperature of $T = 0.9$ MeV. If the excitation energy is known, the temperature provides information about the equation of state. In the Fermi gas model, the temperature varies as the square root of the excitation energy. Also to be noted in this neutron data is that the angular distribution is isotropic for the evaporation neutrons, and is forward peaked for

the higher energy neutrons. These higher energy neutrons emerge at an earlier time in the collision, before equilibrium is established.

Another property of the collision products we would like to know is their angular momentum. It now appears that the products of strongly damped collisions have high angular momentum. Two kinds of experiments give information on this point. The first kind of experiment is to measure the γ-ray multiplicities. At a given excitation energy, γ radiation competes with particle decay more successfully the higher the angular momentum of the state. The gamma decay competes successfully with particle decay near the yrast energy, where E2 transitions to low states in the $(J-2)$ spectrum have lifetimes of the order of 1 ps. Such a state could decay by particle emission only by going to a state of much lower angular momentum, for which there is a large centrifugal barrier. Since the transitions in yrast gamma cascades are E2, the initial angular momentum is about twice the gamma multiplicity. This rule of thumb is only expected to be valid for high multiplicities: when the angular momentum is low there would be two or so gamma rays anyway from the particle bound states. One example recently measured is in the reaction ^{16}O + Ni at 6 MeV/A (ref. [1.8]). The multiplicity of γ rays was measured together with the energy loss of the projectile. Results were:

Energy loss	No. of gamma rays
5–15 MeV	1.5
25–50 MeV	5

For small energy loss, the reaction does not transfer much angular momentum. The strongly damped collisions do have a relatively high multiplicity of gamma rays, indicating substantial angular momentum transfer. Another example is a study [1.9] of ^{20}Ne on Ag at 8.75 MeV/A. The gamma multiplicity for some angles and energies was as high as 15, indicating an angular momentum of 30. Since only about 70 units of angular momentum are brought into the entrance channel, the transfer is very substantial.

A second method for the study of the angular momentum of the products is to measure the angular distribution of a subsequent decay. In favorable cases, this decay distribution will depend on the direction or magnitude of the initial angular momentum vector. The general expression for the decay angular distribution when the decay carries off angular momentum J, M, from the nucleus and also has intrinsic angular momentum K about the decay axis, is given by the Wigner $\mathscr{D}$ function

$$P(\theta) = [\mathscr{D}^{J}_{KM}(\theta)]^2 \,. \tag{1.7}$$

In the case of quadrupole photons for example, $J = 2$ and $K = 1$. If we compare the value of the $\mathscr{D}$ function at 0° and 90°, we find

	$\lvert\mathscr{D}^{2}_{1M}\rvert$	0°	90°
$\lvert M\rvert$ =	2	0	$\frac{1}{2}$
	1	1	$\frac{1}{4}$
	0	0	0

If more particles are emitted at 90° than at 0°, this would be evidence for alignment of the initial state in high M. An example is the reaction ^{16}O + Al at 6.25 MeV/A, where a gamma ray is observed from the $2^+ \rightarrow 0^+$ transition in a ^{12}C product [1.10]. The ratio of γ rays in the reaction plane to γ rays perpendicular to the reaction plane is

$$R = \sigma_{\text{plane}}/\sigma_{\perp} = 2 \,.$$

The authors interpret this as evidence that the polarization of the ^{12}C(2^+) is perpendicular to the reaction plane. Another example is the decay of ^{20}Ne populated in the ^{16}O(^{16}O, ^{12}C)^{20}Ne reaction [1.11]. Certain excited states of ^{20}Ne decay by α emission. Alpha particles have no intrinsic angular momentum, so $K = 0$ and the angular distribution of eq. (7) is the square of a Legendre polynomial. The ratios R obtained in this reaction exceeded 20. Thus the probability of the ^{20}Ne excited state being in the $M = 0$ substate is very small.

With very heavy nuclei, fusion is followed by fission, and the statistical models of fission predict that it is not likely to occur if there is too much angular momentum about the fission axis. The limitation on K then allows information about J and M to be obtained from eq. (1.7). This analysis was made for the reaction Kr on Bi, observing the subsequent fission of the excited Bi nucleus [1.12]. The ratio R is $\sim$20. The authors find that the amount of angular momentum needed in the decaying state to explain this data is a substantial fraction of the angular momentum available in the collision.

Aside. The polarization of the angular momentum transferred in inelastic collisions has been observed directly in the case of atomic collisions with surfaces [1.21]. In this case it can be directly seen that the polarization direction is along $p \times R$, i.e. what one would expect classically from a ball rubbing against another object.

1.2. High energy collisions

There has been much less quantitative reduction of the data on high energy collisions. A qualitative distinction can be made between central

much more spread out than expected from the nucleon–nucleus data. To study collective effects better, it would be very interesting to have more data at lower projectile energies, below the threshold for production with independent particle kinematics. There is now some preliminary emulsion data suggesting that pions may be produced with a high probability in central collisions at energies as low as 100 MeV/A [1.23].

In this survey of experimental heavy ion physics we have discussed only high and low energies, leaving out the medium energy. Experimentally, medium energy is still terra incognita. From a theoretical side, the hydrodynamic development should have its most significant application in this region. To make contact with experiment at this point, we should ask how the behavior exhibited at low and high energies extrapolates. What happens to strongly damped collisions at higher energy? Does the temperature of 30 MeV deduced from the light fragments in 2 GeV/A collisions, fall smoothly to 1–2 MeV at 10 MeV/A collisions?

2. Quantum equations of motion

2.1. *Density matrix formulation*

Continuum mechanics is based on the use of a small set of variables such as density, current, and stress tensor. This is desirable and necessary when dealing with large systems. On the other hand, the most basic formulation of the physics, with quantum mechanics, contains the full degrees of freedom of the many-body system. An important objective is then to reformulate the quantum problem in a way such that the continuum variables are foremost, and approximations resulting in the elimination of other variables can be made. There is a scheme for this reformulation that was developed in the 1940's [2.1]. The starting point is the N-particle Schrödinger equation, which may be written as

$$\mathrm{i}\frac{\partial}{\partial t}\psi(r_1, r_2, \ldots, r_N, t) = \left[-\sum_i \frac{\nabla_i^2}{2m} + \sum_{i<j} v(r_{ij})\right]\psi\,. \tag{2.1}$$

Here ψ is the full wavefunction for the system, and $v(r_{ij})$ is the interaction between particles i and j. Planck's constant will be included in the equation only when making an explicit conversion of units. Next the density matrix is defined,

$$\tilde{\rho}(r_1, \ldots, r_N, r_1' \ldots, r_N', t) = \psi^*(r_1, \ldots, r_N, t)\psi(r_1', \ldots, r_N', t)\,. \tag{2.2}$$

The density matrix will not have any practical value, because the number of variables is twice that of the wavefunction. However, it has the advantage of being a quantity which is observable in principle. The quantum equation of motion can be expressed as an equation for $\tilde{\rho}$. This is the usual Heisenberg form,

$$-\mathrm{i}(\partial/\partial t)\tilde{\rho} = \left[-\sum_i[(\nabla_i^2 - \nabla_i'^2)/2m] + \sum_{i<j}(v(r_{ij}) - v(r_{ij}'))\right]\tilde{\rho}\,. \tag{2.3}$$

We also define a one-body density matrix by writing $r_n = r_n'$ for all but one of the coordinates in eq. (2.2) and integrating over these coordinates,

$$\rho^{(1)}(r_1, r_1', t) = N\int \tilde{\rho}(r_1, r_2, \ldots, r_N, r_1', r_2, \ldots, r_N, t)\,\mathrm{d}r_2 \ldots \mathrm{d}r_N\,. \tag{2.4}$$

If the wavefunction is antisymmetric, it does not matter which coordinate is singled out in this density matrix. In a similar way the two-body density matrix may be defined by integrating out the coordinates of all but two of the particles,

$$\rho^{(2)}(r_1, r_2, r_1', r_2') = N(N-1) \times \int \tilde{\rho}(r_1, r_2, r_3, \ldots, r_N, r_1', r_2', r_3', \ldots, r_N)\,\mathrm{d}r_2 \ldots \mathrm{d}r_N\,. \tag{2.5}$$

To derive the equation of motion for the reduced density matrices, integrate eq. (2.3) over all but n of the coordinates. On the right-hand side, the terms in $v(r_{ij}) - v(r_{ij}')$ obviously vanish if both primed coordinates are set equal to the unprimed coordinates. Also, the term $\nabla_i^2 - \nabla_i'^2$ gives no contribution if the coordinate i is integrated out. This is seen by integrating ∇^2 by parts. The result is the following equation for the n-particle density matrix

$$-\mathrm{i}\frac{\partial}{\partial t}\rho^{(n)}(r_1, \ldots, r_n, r_1', \ldots, r_n', t) = -\sum_{i=1}^{n}\frac{\nabla_i^2 - \nabla_i'^2}{2m}\rho^{(n)} + \sum_{i<j}^{n}(v(r_{ij}) - v(r_{ij}'))\rho^{(n)} \times \sum_{i=1}^{n}\int [v(r_{im}) - v(r_{im}')]\rho^{(n+1)}(r_1, \ldots, r_n, r_m, r_1', \ldots, r_n', r_m')\,\mathrm{d}r_m\,. \tag{2.6}$$

In particular, the equation satisfied by the one-body density matrix is

$$-\mathrm{i}\frac{\partial}{\partial t}\rho^{(1)} = -\frac{\nabla^2 - \nabla'^2}{2m}\rho^{(1)} + \int [v(r, r_2) - v(r', r_2)] \times \rho^{(2)}(r, r_2, r', r_2)\,\mathrm{d}r_2\,. \tag{2.7}$$

The equation for each density matrix involves the density matrix for one additional particle. This set of equations is very analogous to a set of equations for the classical n-particle densities, called the BBGKY hierarchy [2.2]. The goal of theory is to truncate this set of equations at some low order, by making a suitable approximation to the n-particle density matrix in terms of lower order density matrices. However, to my knowledge only the lowest order equation, eq. (2.7), has ever been applied to quantum dynamics.

2.2. *The Wigner function*

The equation of motion can be given a further reformulation to give it the appearance of a classical equation for the phase distribution function. To this end a quantum distribution function is defined as follows:

$$f(p, r) = [1/(2\pi)^3] \int \exp(\mathrm{i}p\cdot x)\rho^{(1)}(r + \tfrac{1}{2}x, r - \tfrac{1}{2}x)\, \mathrm{d}x\,. \tag{2.8}$$

This function contains the same information as the one-body density matrix, since it is nothing more than a Fourier transform. It was first discussed by Wigner [2.3] and is known as the Wigner function.

Exercise. Evaluate the Wigner function for the following wavefunctions:

(a) $\psi = \mathscr{A} \prod^{t} \exp(\mathrm{i}k_i\cdot r_i)$, (b) $\psi = \exp(-\tfrac{1}{2}\nu r^2)$.

In many ways the Wigner function behaves as a classical distribution function. In particular, the basic observables of ordinary density, current, and momentum current are given by the same integrals over f as in classical physics:

$$\rho(r) \equiv \rho^{(1)}(r, r) = \int f(p, r)\, \mathrm{d}\boldsymbol{p}\,, \tag{2.9}$$

$$\boldsymbol{j}(r) \equiv \frac{1}{m}\left(\frac{\boldsymbol{\nabla}' - \boldsymbol{\nabla}}{2\mathrm{i}}\rho^{(1)}\right)_{r=r'} = \int \frac{\boldsymbol{p}}{m} f(p, r)\, \mathrm{d}\boldsymbol{p}\,, \tag{2.10}$$

$$\tau_{ij}(r) = \int p_i v_j f(p, r)\, \mathrm{d}\boldsymbol{p}\,. \tag{2.11}$$

Wigner pointed out in his original paper that there is a limitation on the possibilities of a classical interpretation of f. Namely, the quantum f can be negative in some regions, while the classical f is always non-negative. Fortunately this does not cause any practical difficulties. Even when the integrand is negative in some regions, the integral will be positive if the observable is intrinsically positive.

Aside. In eqs. (2.9–11) an interpretation is given to integrals of f over momentum. The integral of f over coordinate space has an interpretation also. The number of particles emerging from a reaction at a given momentum $\boldsymbol{p}$ is given by

$$\mathrm{d}N/\mathrm{d}\boldsymbol{p} = \lim_{t\to\infty} \int f(p, r, t)\, \mathrm{d}\boldsymbol{r}\,. \tag{2.12}$$

Presumably a reaction theory could be based on this relation and the equation of motion for f [2.4].

The equation (2.7) of motion for the one-body density matrix becomes very similar to a classical equation, when the equation of motion is expressed in terms of the Wigner function. To recast it in this form, the density ρ in eq. (2.7) is expressed as $\rho(r + \frac{1}{2}x, r - \frac{1}{2}x)$ and the equation is integrated over $\boldsymbol{x}$ with $\exp(\mathrm{i}p\cdot x)/(2\pi)^3$. The left-hand side is simply the time derivative of f, and the right-hand side is a complicated expression,

$$\begin{aligned} -\mathrm{i}\frac{\partial}{\partial t} f = &-\frac{1}{2m}\int \frac{\mathrm{d}\boldsymbol{x}}{(2\pi)^3}\left[\nabla_r^2\rho(r, r') - \nabla_{r'}^2\rho(r, r')\right]_{r+x/2,\, r-x/2} \exp(\mathrm{i}p\cdot x) \\ &+ \int \frac{\mathrm{d}\boldsymbol{x}}{(2\pi)^3}\exp(\mathrm{i}p\cdot x)\int \mathrm{d}\boldsymbol{r}''\left[v(r + \tfrac{1}{2}x, r'') - v(r - \tfrac{1}{2}x, r'')\right] \\ &\times \rho^{(2)}(r + \tfrac{1}{2}x, r''; r - \tfrac{1}{2}x, r'')\,. \end{aligned} \tag{2.13}$$

The first term on the right-hand side, the kinetic energy, can be simplified by noting that the expression in brackets is equivalent to the mixed derivative

$$\left[\nabla_r^2\rho(r, r') - \nabla_{r'}^2\rho(r, r')\right]_{r+x/2,\, r-x/2} = 2\nabla_r\cdot\nabla_x\rho(r + \tfrac{1}{2}x, r - \tfrac{1}{2}x)\,. \tag{2.14}$$

With this replacement, the kinetic energy term may be integrated by parts as follows:

$$\begin{aligned} &-\frac{1}{2m}\int \frac{\mathrm{d}\boldsymbol{x}}{(2\pi)^3}\exp(\mathrm{i}p\cdot x)2\nabla_r\cdot\nabla_x\rho(r + \tfrac{1}{2}x, r - \tfrac{1}{2}x) \\ &\quad = \frac{\nabla_r}{m}\cdot\int \frac{\mathrm{d}\boldsymbol{x}}{(2\pi)^3}(\mathrm{i}p)\exp(\mathrm{i}p\cdot x)\rho(r + \tfrac{1}{2}x, r - \tfrac{1}{2}x) \\ &\quad = \mathrm{i}[(p\cdot\nabla_r/m]f(p, r)\,. \end{aligned} \tag{2.15}$$

Equation (2.13) then has the appearance of the classical Boltzmann equation, but with a rather peculiar collision term,

$$(\partial/\partial t)f + v\cdot\nabla f = \mathrm{i}\int [\mathrm{d}x/(2\pi)^3]\exp(\mathrm{i}p\cdot x)\int \mathrm{d}r''[v(r+\tfrac{1}{2}x, r'') - v(r-\tfrac{1}{2}x, r'')] \times \rho^{(2)}(r+\tfrac{1}{2}x, r''; r-\tfrac{1}{2}x, r'') . \tag{2.16}$$

This is as far as the reduction can be carried in full generality. This equation requires prior knowledge of the two-body density matrix $\rho^{(2)}$, and so is not very useful as it stands. To make the equation closed, the two-body density matrix can be approximated by the product of one-body density matrices:

$$\rho^{(2)}(r_1, r_2; r_1', r_2') = \rho(r_1, r_1')\rho(r_2, r_2') - \rho(r_1, r_2')\rho(r_2, r_1') . \tag{2.17}$$

This is the Hartree–Fock approximation. If only the first term in eq. (2.17) is kept, the Hartree theory results. In this approximation, a local one-body potential can be defined,

$$U(r) = \int \mathrm{d}r_2\rho(r_2, r_2)v(r, r_2) .$$

The equation of motion of the particles is identical to that for particles in an external potential $U(r)$. The second term in eq. (2.17), the exchange density, is to be interpreted to include spin and isospin as well as spatial coordinates in the coordinates r_i. Inclusion of exchange causes some practical difficulties in the theory because the corresponding one-body potential is non-local. However, a local approximation can be made to the exchange and still preserve the main physics as was shown by Negele and Vautherin [2.5]. The exchange contribution to the spatial integral in eq. (2.16) is written as:

$$(U\rho)_{\mathrm{exch}} = \int \mathrm{d}r_2 v(r_1', r_2)\rho(r_1, r_2)\rho(r_2, r_1') . \tag{2.18}$$

In this integral the density $\rho(r_1, r_2)$ is expanded about the point $r_2 = r_1'$,

$$\rho(r_1, r_2) = \rho(r_1, r_1') + (r_2 - r_1')\cdot\nabla'\rho + \tfrac{1}{2}\sum_{ij}(r_2 - r_1')_i \times (r_2 - r_1')_j \nabla_i'\nabla_j'\rho + \cdots .$$

Also, the density matrix $\rho(r_2, r_1')$ in eq. (2.18) is replaced by its value in the infinite Fermi gas.

Then the exchange integral becomes:

$$(U\rho)_{\mathrm{exch}} = \rho^{(1)}(r_1, r_1')\left(\int \rho_{\mathrm{FG}} v\,\mathrm{d}r\right) - \nabla'\rho\cdot\int \rho_{\mathrm{FG}} r v\,\mathrm{d}r + \nabla^2\rho\left(\int \tfrac{1}{3}r^2\rho_{\mathrm{FG}} v\,\mathrm{d}r\right) . \tag{2.19}$$

The first term is just an ordinary local potential and can be included with the Hartree potential. This approximation was introduced by Slater to atomic calculations. The third term depends on the Laplacian of the density matrix and can be included with the kinetic energy. The particles will then have an effective mass different from their free mass. The second term in eq. (2.19) vanishes in the Fermi gas approximation, but has been retained because the principle of Galilean invariance will require that it be included if the term $\nabla^2\rho$ is kept in the theory. In the further exposition of the theory, we will drop both of these terms.

With a local approximation to the direct and exchange potentials,

$$U(r) = \int \mathrm{d}r_2\rho(r_2)v(r, r_2) + \int \rho_{\mathrm{FG}} v\,\mathrm{d}r_2 ,$$

the equation of motion becomes,

$$\frac{\partial}{\partial t}f + v\cdot\nabla f = \mathrm{i}\int \frac{\mathrm{d}x}{(2\pi)^3}\exp(\mathrm{i}p\cdot x)[U(r+\tfrac{1}{2}x) - U(r-\tfrac{1}{2}x)] \times \rho(r+\tfrac{1}{2}x, r-\tfrac{1}{2}x) . \tag{2.20}$$

The many-body physics enters only through the relation of the potential U to the density.

One more approximation reduces the equation to completely classical form. This is to make a power series expansion of the one-body potential,

$$U(r+\tfrac{1}{2}x) = U(r) + \tfrac{1}{2}x\cdot\nabla U + \cdots , \tag{2.21}$$

keeping only the lowest terms. The integral over the potential then becomes

$$\begin{aligned} &\mathrm{i}\int \mathrm{d}x\exp(\mathrm{i}p\cdot x)[U(r+\tfrac{1}{2}x) - U(r-\tfrac{1}{2}x)]\rho(r+\tfrac{1}{2}x, r-\tfrac{1}{2}x) \\ &\quad\approx \mathrm{i}\int \mathrm{d}x\exp(\mathrm{i}p\cdot x)x\cdot\nabla U\rho^{(1)} \\ &\quad= \mathrm{i}\nabla U\cdot\int \mathrm{d}x\,(1/\mathrm{i})\nabla^p\exp(\mathrm{i}px)\rho^{(1)} \\ &\quad= \nabla U\cdot\nabla^p f(p, r) . \end{aligned} \tag{2.22}$$

The equation for f then becomes

$$(\partial/\partial t)f + v\cdot\nabla^x f - \nabla U\cdot\nabla^p f = 0\,. \tag{2.23}$$

The last term may be interpreted as the rate of change in distribution function in momentum space due to a gradient of a potential, i.e. the acceleration of particles due to a force. In this equation we have lost such quantum mechanical effects as the penetration of particles under a barrier.

Equation (2.23), with the potential U determined self consistently from the density, is known as the Vlasov equation [2.6]. It was first used to describe electrons and ions in plasmas. The dynamics are completely classical: the only strong quantum effect is that the density matrix must not violate the Pauli exclusion principle. The initial density matrix satisfies this constraint if it is constructed from an antisymmetric wave-function. The usual way to do this is to make a Slater determinant of orthogonal wave-functions. Once properly constructed, the density matrix will continue to satisfy the Pauli principle as time goes on. From a quantum point of view, this comes about because all the particles are governed by the same Hamiltonian equation. Since the Hamiltonian generates a unitary transformation on the single-particle wave-functions, the initial orthogonality of these wave-functions is preserved for all time, and thus the Pauli principle continues to be satisfied. From the classical point of view, eq. (2.23) is nothing more than Liouville's equation for a single particle. Liouville's equation produces incompressible flow of particles in phase space. Thus if we start with a density that satisfies a classical version of the Pauli principle ($f \leqslant 1/h^3$), it will continue to satisfy this at later times.

2.3. *Conservation laws*

In making approximations on a theory of dynamics the most important properties to be retained are the fundamental conservation laws of mass, energy, and momentum. The Vlasov equation does satisfy these laws, and so is an acceptable theory at this basic level. To show that mass is conserved, eq. (2.23) is integrated over momentum:

$$\int \mathrm{d}\boldsymbol{p}[(\partial/\partial t)f + v\cdot\nabla^x f - \nabla U\cdot\nabla^p f] = 0\,. \tag{2.24}$$

The last term is the integral of a gradient, which vanishes because f goes to zero for large values of $\boldsymbol{p}$. The first two terms may be expressed with the help of eqs. (2.9) and (2.10) as

$$(\partial/\partial t)\int \mathrm{d}\boldsymbol{p} f + \nabla^x\cdot\int \mathrm{d}\boldsymbol{p} v f = (\partial/\partial t)\rho + \nabla^x\cdot j = 0\,. \tag{2.25}$$

This is the usual equation for the local conservation of mass or particle number. The momentum conservation law is obtained by integrating the Vlasov equation over $\int \mathrm{d}\boldsymbol{p}\,\boldsymbol{p}$. The result is

$$\int \mathrm{d}\boldsymbol{p}\,\boldsymbol{p}[(\partial/\partial t)f + v\cdot\nabla^x f - \nabla U\cdot\nabla^p f] = 0$$

$$= m(\partial \boldsymbol{j}/\partial t) + \nabla_i^x\cdot[\tau_{ij} + \delta_{ij}(U\rho - V)] = 0\,, \tag{2.26}$$

where τ_{ij} is given by eq. (2.11), and V is the potential energy per unit volume, related to U by $\delta V/\delta\rho = U$. The first term is rate of change of momentum, and the second term may be interpreted as the divergence of the momentum flux Π_{ij},

$$\Pi_{ij} = \tau_{ij} + \delta_{ij}(U\rho - V)\,. \tag{2.27}$$

The equation can be recast into a standard hydrodynamic form by defining the pressure tensor,

$$P_{ij} = \Pi_{ij} - m j_i j_j/\rho\,. \tag{2.28}$$

Substituting eq. (2.28) into eq. (2.26) and making use of the equation of continuity, the following equation can be derived,

$$\rho(\partial \boldsymbol{u}/\partial t) + \rho\boldsymbol{u}\cdot\nabla\boldsymbol{u} = -(1/m)\nabla_i\cdot P_{ij}\,, \qquad \text{where } \boldsymbol{u} = \boldsymbol{j}/\rho\,. \tag{2.29}$$

This equation would be the Navier–Stokes equation of hydrodynamics if the anisotropic part of the pressure tensor happened to have the form

$$\mu(\nabla_i u_j + \nabla_j u_i)\,.$$

The pressure tensor will be isotropic if the distribution function is concentrated in momentum space, for then

$$\tau_{ij} \approx m\rho u_i u_j\,.$$

This possibility is realized in the distribution function of the condensate of a many-boson system. Thus bosons will obey standard classical hydrodynamics.

Aside. For the many-boson system, irrotational hydrodynamics can be derived quite directly [2.7, 2.8] from the wavefunction

$$\psi = \prod_i \phi(r_i)\,.$$

Here ϕ is the single particle wavefunction of a boson. There are two degrees of freedom in the (complex) wavefunction, and these are represented in terms of real function $\chi(r, t)$, $R(r, t)$,

$$\phi(r, t) = \exp[\mathrm{i}\chi(r, t)]R(r, t)\phi_0(r)\,,$$

where ϕ_0 satisfies a time-independent Schrödinger equation. Substituting the above in the Schrödinger equation, and separating real and imaginary parts, one finds two equations. One of these is the equation of continuity and the other is an equation of motion involving a scalar pressure. The pressure has the form

$$P = U\rho - R\phi_0(\hbar^2/2m)\nabla^2 R\phi_0 .$$

Quantum physics only enters by the presence of the second term in pressure. Since the velocity field is proportional to the gradient of the scalar χ, the hydrodynamics will be irrotational.

In general, τ_{ij} will depend on the previous history of the system as well as on $v_i v_j$, and will not be isotropic even in the frame travelling with velocity v_i. Fluid behavior is possible only if isotropy in this frame occurs. This can happen if the system has enough time to relax thermally, or if the residual interaction between particles is attractive. The latter possibility is realized in the superfluid phase of some systems.

For finite systems in equilibrium, the momentum flux Π_{ij} vanishes if the system has no angular momentum. This implies that the momentum distribution cannot have any quadrupole moment. The fact that τ_{ij} must be isotropic in equilibrium has non-trivial consequences, for example in the structure of deformed nuclei. In the shell model of deformed nuclei, orbits are preferentially filled which have maximum extension along some axis. The valence orbits also have the highest momentum, so the momentum will also be highest along the preferred axis. In the harmonic oscillator model of the orbits, there is complete symmetry in r and p space. The isotropy in p space can be restored by rescaling the length parameters of the oscillators. But the scale transformation which produces isotropy in p space doubles the anisotropy, or quadrupole deformation, in r space. This argument, showing that quadrupole moments are double the valence contribution, was first given by Mottelson. Similar considerations may be made for the equilibrium structure of rapidly rotating nuclei.

Except for special cases, the solutions to the Vlasov equation are not available. One trivial case occurs if the potential U vanishes. Then the solution to eq. (2.23) is simply

$$f(p, r, t) = f_0[p, r - (p/m)t] .$$

Obviously, the particles simply propagate freely. For small amplitude disturbances in an infinite medium, the solution to the Vlasov equation was first given by Landau. He first developed the theory for the plasma [2.9] and then for liquid ^{3}He (ref. [2.10]). For our purposes the most important

feature of the solution is the possibility of two types of behavior, dissipative and non-dissipative, depending on the character of the self-consistent potential U. This will be considered in greater detail in sect. 5.

2.4. The quantum mechanical sum rules

Another situation that can be easily analyzed with the Vlasov equation is the short-time behavior of a system subject to an impulsive force. Suppose the system starts out in equilibrium, with a static distribution function given by $f_0(p, r)$. At some time t_0 a potential is applied to the system of the form

$$V_{\text{ext}} = V(r)\delta(t - t_0) .$$

The equation of motion of the system is

$$(\partial/\partial t)f + v\cdot\nabla^x f - \nabla U\cdot\nabla^p f = \nabla V_{\text{ext}}\cdot\nabla^p f . \tag{2.30}$$

Because of the δ-function potential, there is a discontinuity in f at $t = t_0$. If the external potential is weak, this is

$$\begin{aligned} f &= f_0 && \begin{cases} t < t_0 \\ t = t_0 + \varepsilon . \end{cases} \\ &= f_0 + \nabla V\cdot\nabla^p f_0 \end{aligned} \tag{2.31}$$

Thus the self-consistent potential U does not play any role immediately after t_0. The current immediately after t_0 is given by the integral of eq. (2.31) over $\int \mathrm{d}p\, \boldsymbol{p}/m$:

$$\boldsymbol{j} = \int \mathrm{d}\boldsymbol{p}(\boldsymbol{p}/m)f|_{t=t_0+\varepsilon} = \nabla V\cdot\int \mathrm{d}\boldsymbol{p}(\boldsymbol{p}/m)\nabla^p f_0 = -\boldsymbol{\nabla} V\rho_0 .$$

The equation of continuity, eq. (2.25) then implies

$$\dot{\rho}|_{t=t_0+\varepsilon} = -\boldsymbol{\nabla}\cdot\rho_0\boldsymbol{\nabla} V . \tag{2.32}$$

The analogous equation in quantum mechanics is an energy-weighted sum rule. This may be shown by following the same derivation in the wavefunction language of quantum mechanics. The initial ground state wavefunction will be represented by ψ_0, and the excited states by ψ_n. The equation of motion is

$$\mathrm{i}(\partial\psi/\partial t) = H\psi , \tag{2.33}$$

with

$$H = H_0 + V(r)\delta(t - t_0) \qquad \text{and} \qquad H_0\psi_n = E_n\psi_n . \tag{2.34}$$

Then if the potential $U(r)$ is sufficiently weak, the solution to eq. (2.33) for $t > t_0$ is

$$\psi = \exp[-iE_0t]\psi_0 + \sum_n \frac{\langle\psi_n|V(r)|\psi_0\rangle}{i} \times \exp[-iE_nt + i(E_n - E_0)t_0]\psi_n . \tag{2.35}$$

This wave-function will be used to calculate the rate of change of density, $\dot{\rho}$. The density is given by

$$\langle\psi|\rho|\psi\rangle = \rho_0 + \sum_n \langle\psi_0|V(r)|\psi_n\rangle\langle\psi_n|\hat{\rho}|\psi_0\rangle 2\sin(E_0 - E_n)(t - t_0) .$$

The derivative of this with respect to time, evaluated at $t = t_0$, is

$$\langle\dot{\rho}\rangle_{t_0} = 2\sum_n (E_0 - E_n)\langle\psi_0|V|\psi_n\rangle\langle\psi_n|\hat{\rho}|\psi_0\rangle . \tag{2.36}$$

A closed expression for the left-hand side may be found by using the identity

$$(E_n - E_0)\langle\psi_0|V(r)|\psi_n\rangle = \langle\psi_n|[H, V]|\psi_0\rangle = \langle\psi_0|\frac{1}{2m}(\nabla^2 V) + \frac{(\nabla V)\cdot\boldsymbol{\nabla}}{m}|\psi_n\rangle . \tag{2.37}$$

Inserting eq. (2.37) in eq. (2.36), and using closure on the sum over states n, we find

$$\langle\dot{\rho}\rangle_{t_0} = -\langle\psi_0|\left(\frac{\nabla^2 V}{m} + 2\frac{\nabla V\cdot\boldsymbol{\nabla}}{m}\right)\hat{\rho}|\psi_0\rangle = -\frac{\nabla\cdot\langle\psi_0|\hat{\rho}|\psi_0\rangle\nabla V}{m} . \tag{2.38}$$

This is identical to eq. (2.32). These sum rules were introduced by Fallieros [2.11] and by Noble [2.12]. They reduce to the ordinary Thomas–Reiche–Kuhn type sum rule by integrating both sides with $\int dr V(r)$,

$$\sum_n (E_n - E_0)\langle\psi_0|V(r)|\psi_n\rangle^2 = -\tfrac{1}{2}\int dr V(r)(\nabla\cdot\rho_0\nabla V)/m = \int (\rho_0/2m)(\nabla V)^2\, d\mathbf{r} . \tag{2.39}$$

If it should happen that one state exhausts the sum rule, then its transition density must be

$$\langle\psi_n|\hat{\rho}|\psi_0\rangle = -(\nabla\cdot\rho\nabla V)/2m(E_n - E_0)\langle\psi_0|V|\psi_n\rangle . \tag{2.40}$$

In classical terms, the equivalent statement would be that if the motion associated with the velocity field ∇V were sinusoidal, then the amplitude of the density change has to be given by $\dot{\rho}$ divided by the frequency.

2.5. Evolution of the distribution function

While it is not possible to integrate the Vlasov equation in general, some insight may be gained by expanding the solution for small intervals of time. The starting point again is an equilibrium solution f_0, which is perturbed by the impulsive potential

$$V(r)\delta(t - t_0) . \tag{2.41}$$

We have so far obtained the distribution immediately after time t_0, eq. (2.31). We add to this a power series in the time $t - t_0$, as follows:

$$f = f_0 + \nabla V\cdot\nabla^p f_0 + (t - t_0)f_1 + \tfrac{1}{2}(t - t_0)^2 f_2 + \cdots . \tag{2.42}$$

The above is inserted in eq. (2.23) and powers of t are collected together. The terms involving only f_0 cancel because it is an equilibrium solution:

$$v\cdot\nabla f_0 - \nabla U\cdot\nabla^p f_0 = 0 . \tag{2.43}$$

The remaining terms independent of t satisfy

$$f_1 + v\cdot\nabla(\nabla V)\cdot\nabla^p f_0 - \nabla U\cdot\nabla^p\nabla V\cdot\nabla^p f_0 = 0 . \tag{2.44}$$

This can be simplified by using eq. (2.43),

$$\begin{aligned} f_1 &= -v_i\nabla_i\nabla_j V\cdot\nabla_j^p f_0 + (\nabla_j V)\nabla_j^p v_i\nabla_i f_0 \\ &= -v_i(\nabla_i\nabla_j V)\nabla_j^p f_0 - v_i(\nabla_j V)\nabla_i\nabla_j^p f_0 + (1/m)\nabla_i V\cdot\nabla_i f_0 \\ &\quad + (\nabla_i V)v_j\nabla_j\nabla_j^p f_0 \\ &= -v_i(\nabla_i\nabla_j V)\nabla_j^p f_0 + (1/m)\nabla_i V\cdot\nabla_i f_0 . \end{aligned} \tag{2.45}$$

To avoid confusion, the Cartesian indices are explicitly shown on the vectors where there can be ambiguity. Also, the gradients within parentheses act only on the function within the parentheses. The result for the linear dependence of the distribution function on time becomes more transparent if the power series is expressed as a power series in the argument of f_0. Thus,

$$\begin{aligned} f_0 &+ \nabla V\cdot\nabla^p f_0 - v_i(\nabla_i\nabla_j V)\nabla_j^p f_0 t + (1/m)\nabla_i V\cdot\nabla_i f_0 t \\ &= f_0[p + \nabla V - v_i(\nabla_i\nabla_j V)t, r + (\nabla_i V/m)t] . \end{aligned} \tag{2.46}$$

From examination of the spatial argument of this distribution function it may be seen that, to first order in t, the distribution function is being

displaced at a locally constant velocity. The magnitude of the velocity is exactly what should be expected from the impulsive potential. A simple example is the distribution function resulting from a uniform force,

$$V(r) = -zI\delta(t - t_0) . \tag{2.47}$$

Equation (2.46) becomes

$$f(p, r, t) = f_0[p - I, r - (I/m)t] . \tag{2.48}$$

The distribution function now has uniform translational motion. The solution (2.48) is exact if U is a self-consistent potential. Assuming eq. (2.48) to be a solution, a self-consistent potential depending only on density must depend on time as

$$U(r, t) = U_0[r - (I/m)t] , \tag{2.49}$$

and eq. (2.23) is satisfied identically.

Exercise. Show explicitly that eq. (2.48) solves eq. (2.23).

When a solution is transformed by replacing r with $r - vt$ and the result is also a solution, the theory is said to be Galilean invariant. This invariance is a very useful property to have when studying long-wavelength excitations. Suppose the system is undergoing some motion that is smooth, but not necessarily uniform. Then the motion may be regarded as uniform translation for local regions in the system, to some approximation. Thus the actual solution will be only slightly different from the ground state, and an expansion of the motion in this small parameter of the non-uniformity can be contemplated.

Equation (2.46) shows that for non-uniform motion the momentum dependence of the distribution function changes in first order in t. The significance of this can be seen easily by example. Suppose that V were a potential that applied a uniform compression to the medium, i.e.

$$V = \tfrac{1}{2}\alpha r^2 . \tag{2.50}$$

Then the velocity would be directed radially, and we would expect the density to increase uniformly with time. With the potential (2.50) the momentum argument for f has the form $\boldsymbol{p}[1 - (\alpha/m)t] + \alpha\boldsymbol{r}$. Integrating over momentum to get the density we find

$$\begin{aligned}\int \mathrm{d}\boldsymbol{p} f(p, r, t) &= \{1/[1 - (\alpha/m)t]^3\} \int \mathrm{d}p' f_0(p', r) \\ &= \rho_0/[1 - (\alpha/m)t]^3 .\end{aligned} \tag{2.51}$$

Thus the increase in density comes about from the expansion of the distribution function in momentum space. It is also of interest to examine the effect of a shear field on the distribution function, for example the potential $V = z^2 - \frac{1}{2}x^2 - \frac{1}{2}y^2$. The distribution function which started out spherically symmetric in the argument p, now acquires a quadrupole distortion. Later, an equation will be needed for the time rate of change of the momentum flux, τ_{ij}. If eq. (2.46) is integrated with $p_i v_j$, and the result is expanded to first order in time, we find

$$\begin{aligned}(\mathrm{d}/\mathrm{d}t)\tau_{ij} &= \int \mathrm{d}\boldsymbol{p}(p_i p_j/m) p_k \nabla_e^p f_0 \nabla_k \nabla_e f_0 \\ &= -(\langle p^2\rangle\rho/3m)(\nabla_i v_j + \nabla_j v_i) - \delta_{ij}(\langle p^2\rangle\rho/3m)\nabla\cdot v ,\end{aligned} \tag{2.52}$$

assuming f_0 to be isotropic. This shows explicitly how the anisotropy develops from a flow that contains shear.

Exercise. Determine the distribution function of an infinite uniform system to second order in t when the system is subjected to the field $V = \mathrm{Re}\exp(\mathrm{i}kx)$ initially.

Exercise. Determine how the Vlasov equation is modified if the residual interaction has an additional term with a quadratic dependence on relative momentum.

---

3. Small amplitude oscillations in finite systems

The theory of small amplitude oscillations in finite systems governed by the Vlasov equation has a tractable form. Without making unreasonable approximations, a closed expression may be given for the frequency of small amplitude oscillations. This expression has the appearance of Rayleigh's variational principle, with a certain explicit form for the potential energy function. The starting point of the derivation is the Vlasov equation,

$$(\partial/\partial t)f + \boldsymbol{v}\cdot\nabla f - \nabla U\cdot\nabla^p f = 0 . \tag{3.1}$$

In this equation and in the rest of the section, we omit the superscript on the spatial gradient operator. Solutions to the Vlasov equation will be represented in the form

$$f = f_0 + f_u + f_g . \tag{3.2}$$

Here f_0 is the equilibrium solution, which does not depend on time. The time dependence is contained in f_u and f_g, which are assumed small compared with f_0. The f_u is odd under the transformation $\boldsymbol{p} \to -\boldsymbol{p}$, and f_g is even under this transformation. Thus, the current will depend only on f_u

and the density fluctuation will depend only on f_g. We next express f_u in terms of a vector field $\boldsymbol{u}$,

$$f_u = -\boldsymbol{u}\cdot\nabla^p f_0 \,. \tag{3.3}$$

If u is allowed to depend on both position and momentum, there is no loss of generality in writing f_u in the form eq. (3.3). However, we shall assume that u depends only on position to derive a manageable formula. Substituting eq. (3.2) in eq. (3.1), we obtain two separate equations for the time derivatives of f_u and f_g. The equation for f_g has only the terms even in $\boldsymbol{p}$, and is

$$(\partial f_g/\partial t) - v\cdot\nabla\boldsymbol{u}\cdot\nabla^p f_0 + \boldsymbol{u}\cdot\nabla U_0\cdot\nabla^p\nabla^p f_0 = 0 \,. \tag{3.4}$$

Here U_0 is the time-dependent part of the potential field U. Other terms in this equation involving only f_0 have dropped out because of the equilibrium condition,

$$v\cdot\nabla f_0 - \nabla U_0\cdot\nabla^p f_0 = 0 \,. \tag{3.5}$$

We have also assumed that the potential U depends only on f_0 and f_g. It is useful to rewrite eq. (3.4) by carrying out the gradient operation in the middle term,

$$v_i\nabla_i u_j\nabla_j^p f_0 = v_i(\nabla_i u_j)\nabla_j^p f_0 + v_i u_j\nabla_j^p\nabla_i f_0 \,. \tag{3.6}$$

The parentheses in the first term indicated that the gradient only acts on the function within the parentheses. The Cartesian indices on the vectors are also explicitly written out where confusion is possible. Also note that the equilibrium condition, eq. (3.5), implies the following identity:

$$\begin{aligned} &u_i\nabla_i^p(v_j\nabla_j f_0 - \nabla_j U_0\nabla_j^p f_0) \\ &\quad = u_i v_j\nabla_j\nabla_i^p f_0 + u\cdot\nabla f_0/m - u_i\nabla_j U_0\nabla_i^p\nabla_j^p f_0 = 0 \,. \end{aligned} \tag{3.7}$$

Combining eqs. (3.4), (3.6), and (3.7), the equation for f_g becomes

$$\partial f_g/\partial t - v_i(\nabla_i u_j)\nabla_j^p f_0 + u\cdot\nabla f_0/m = 0 \,. \tag{3.8}$$

We can check immediately that our distribution function satisfies the equation of continuity. The current is related to the f_u defined in eq. (3.3) by

$$\boldsymbol{j} = \int \mathrm{d}\boldsymbol{p}\boldsymbol{v}f_u = -\int \mathrm{d}\boldsymbol{p}(\boldsymbol{p}/m)u\cdot\nabla^p f_0 = \boldsymbol{u}\int \mathrm{d}\boldsymbol{p} f_0 = \boldsymbol{u}\rho \,. \tag{3.9}$$

The time derivative of the density may be found by integrating eq. (3.8) over momentum,

$$\dot\rho = \int \mathrm{d}\boldsymbol{p}\,\partial f_g/\partial t = \int \mathrm{d}p[v_i(\nabla_i u_j)\nabla_j^p f_0 - \boldsymbol{u}\cdot\nabla f_0] = -(\nabla\cdot\boldsymbol{u})\rho - \boldsymbol{u}\cdot\nabla\rho \,. \tag{3.10}$$

The right-hand side of this equation is just the negative divergence of the current defined in eq. (3.9). This proves the assertion.

The equation for the time derivative of f_u we write as

$$\partial f_u/\partial t + \boldsymbol{v}\cdot\nabla f_g - \nabla U_0\cdot\nabla^p f_g - [\nabla(\delta U/\delta\rho)\delta\rho]\cdot\nabla^p f_0 = 0 \,. \tag{3.11}$$

The last term expresses the dependence of the one-body potential on the distribution function, which we have limited to a dependence on the ordinary density,

$$\rho = \rho_0 + \delta\rho \,; \qquad \delta\rho = \int \mathrm{d}p f_g = -\int \mathrm{d}t[(\nabla\cdot u)\rho_0 + u\cdot\nabla\rho_0] \,. \tag{3.12}$$

Next take the time derivative of eq. (3.11) and substitute from eq. (3.8). This gives the following equation:

$$\begin{aligned} &-\ddot u\cdot\nabla^p f_0 + v_i\nabla_i[v_j(\nabla_j u_k)\nabla_k^p f_0 - u_j\nabla_j f_0] - \nabla_i U_0\nabla_i^p \\ &\quad\times [v_j(\nabla_j u_k)\nabla_k^p f_0 - u_j\nabla_j f_0] - [\nabla(\delta U/\delta\rho)\delta\dot\rho]\cdot\nabla^p f_0 = 0 \,. \end{aligned} \tag{3.13}$$

To simplify this equation, we first carry through all the gradient operators. The result is:

$$\begin{aligned} &-\ddot u\cdot\nabla^p f_0 + v_i v_j(\nabla_i\nabla_j u_k)\nabla_k^p f_0 + v_i v_j(\nabla_j u_k)\nabla_k^p\nabla_i f_0 - v_i(\nabla_i u_j)\nabla_j f_0 \\ &\quad - v_i u_j\nabla_i\nabla_j f_0 - (\nabla_i U_0)(\nabla_i u_k)\nabla_k^p f_0 - (\nabla_i U_0)v_j(\nabla_j u_k)\nabla_k^p\nabla_i^p f_0 \\ &\quad + u_j\nabla_j(\nabla_i U_0)\nabla_i^p f_0 - u_j(\nabla_j\nabla_i U_0)\nabla_i^p f_0 \\ &\quad - [\nabla(\delta U/\delta\rho)\delta\dot\rho]\cdot\nabla^p f_0 = 0 \,. \end{aligned} \tag{3.14}$$

Making use of the equilibrium condition eq. (3.5) again, the seventh term can be replaced by

$$\begin{aligned} v_j(\nabla_j u_k)\nabla_k^p\nabla_i U_0\nabla_i^p f_0 &= v_j(\nabla_j u_k)\nabla_k^p v\cdot\nabla f_0 \\ &= v_j(\nabla_j u_k)\nabla_k f_0 + v_j v_i(\nabla_j u_k)\nabla_k^p\nabla_i f_0 \,. \end{aligned} \tag{3.15}$$

In a similar way, the eighth term can be replaced by

$$u_j\nabla_j(\nabla_i U_0)\nabla_i^p f_0 = u_i v_j\nabla_i\nabla_j f_0 \,. \tag{3.16}$$

The result for eq. (3.14) is

$$-\ddot{u}\cdot\nabla^p f_0 + v_i v_j(\nabla_i\nabla_j u_k)\nabla^p_k f_0 - 2v_i(\nabla_i u_j)\nabla_j f_0 - [\nabla(\delta U/\delta\rho)\delta\dot{\rho}]\cdot\nabla^p f_0 - (\nabla_i U_0)(\nabla_i u_k)\nabla^p_k f_0 - u_j(\nabla_j\nabla_i U_0)\nabla^p_i f_0 = 0\,. \tag{3.17}$$

This equation looks complicated but its structure is not difficult to understand. It is a simple second order differential equation in time, so the solutions can be expanded in eigenfrequencies. The scale for the frequencies is fixed by the remaining terms. The second term is quadratic in velocity and second order in space derivatives. The fourth term contains the effect of the time varying part of the central field. The remaining terms, which depend on the spacial gradient of U_0 or f_0, contain surface effects such as surface tension.

We next reduce the equation by multiplying eq. (3.17) by $\boldsymbol{p}_\alpha$ and integrating over momentum. The terms involving $\nabla^p f_0$ can be simplified by integrating by parts. We find

$$\ddot{u}_\alpha\rho - (\nabla_i\nabla_j u_\alpha)\int v_i v_j f_0\,\mathrm{d}p - 2(\nabla_i u_j)\int \mathrm{d}p v_\alpha v_i\nabla_j f_0 - 2(\nabla_i\nabla\cdot u)\int v_i v_\alpha f_0\,\mathrm{d}p + [\nabla_\alpha(\delta U/\delta\rho)\delta\dot{\rho}]\rho + (\nabla_i U_0)(\nabla_i u_\alpha)\rho + u_j(\nabla_j\nabla_\alpha U_0)\rho = 0\,. \tag{3.18}$$

Let us assume that the equilibrium state is isotropic. Then the integrals in eq. (3.18) can be expressed

$$\int \mathrm{d}p\, p_i p_j f_0 = \delta_{ij}\tfrac{1}{3}\langle p^2\rangle\rho_0 = \kappa\delta_{ij} \tag{3.19}$$

Let us also expand $\delta\rho$ according to eq. (3.12). Then eq. (3.18) becomes

$$\ddot{u}_\alpha\rho - \kappa\nabla^2 u_\alpha - [2\kappa + (\delta U/\delta\rho)\rho^2]\nabla_\alpha(\nabla\cdot u) - 2\nabla_\alpha u_i\nabla_i\kappa - \rho\nabla_\alpha(\delta U/\delta\rho)(\nabla\cdot u\rho_0 + u\cdot\nabla\rho_0) + \nabla_i u_\alpha(\nabla_i U_0)\rho + u_j(\nabla_j\nabla_\alpha U_0)\rho = 0\,. \tag{3.20}$$

If we return to consideration of the infinite medium, the terms involving gradients of ρ_0 and U_0 vanish. The equation is then the usual one describing elastic waves, with

$$\lambda = (\delta U/\delta\rho)\rho^2 + \langle p^2\rangle\rho/3m \qquad \text{and} \qquad \mu = \langle p^2\rangle\rho/3m\,. \tag{3.21}$$

The surface terms are not easy to handle, so we shall further simplify the equation by multiplying by u_α, summing over α and integrating over space. If we assume that the motion has a sinusoidal time dependence with frequency ω, eq. (3.14) becomes

$$-\omega^2\int \mathrm{d}r u\cdot u\rho - \int \mathrm{d}r\kappa u_\alpha\nabla^2 u_\alpha - \int \mathrm{d}r 2\kappa u_\alpha\nabla_\alpha(\nabla\cdot u) - 2\int \mathrm{d}r u_\alpha(\nabla_\alpha u_i)\nabla_i\kappa + \int \mathrm{d}r u_\alpha[\nabla_\alpha(\delta U/\delta\rho)\delta\dot{\rho}]\rho + \int \mathrm{d}r u_\alpha(\nabla_i U_0)(\nabla_i u_\alpha)\rho + \int \mathrm{d}r u_\alpha u_j(\nabla_j\nabla_\alpha U_0)\rho = 0\,. \tag{3.22}$$

We further assume at this point that $\boldsymbol{u}$ is the gradient of a scalar field, so that we may replace $\nabla_i u_\alpha$ by $\nabla_\alpha u_i$. The fourth, fifth, and sixth terms in eq. (3.22) can then be integrated by parts as follows:

$$-2\int \mathrm{d}r u_\alpha(\nabla_i u_\alpha)\nabla_i\kappa = 2\int \mathrm{d}r(\nabla_\alpha u_i)^2\kappa + 2\int \mathrm{d}r\kappa u_\alpha\nabla_\alpha(\nabla\cdot u)\,;$$

$$\int \mathrm{d}r u_\alpha[\nabla_\alpha(\delta U/\delta\rho)\delta\dot{\rho}]\rho = \int \mathrm{d}r(\delta\dot{\rho})^2(\delta U/\delta\rho)\,;$$

$$\int \mathrm{d}r u_\alpha(\nabla_i U_0)\rho\nabla_\alpha u_i = -\int \mathrm{d}r(\nabla_i U_0)u_i\delta\dot{\rho} - \int \mathrm{d}r(\nabla_\alpha\nabla_i U_0)u_i u_\alpha\rho\,.$$

The result of these manipulations is

$$-\omega^2\int \mathrm{d}r\rho u\cdot u + \int \mathrm{d}r\kappa[2(\nabla_\alpha u_i)^2 - u_\alpha\nabla^2 u_\alpha] + \int \mathrm{d}r(\delta\dot{\rho})^2(\delta U/\delta\rho) - \int \mathrm{d}r(\nabla_i U_0)u_i\delta\dot{\rho} = 0\,. \tag{3.23}$$

This equation may be cast into the form of Rayleigh's variational principle by solving for ω^2. The equation is

$$\omega^2 = (I_u + I_v)/I_M\,, \tag{3.24a}$$

where the integrals I are defined

$$I_M = \tfrac{1}{2}\int \mathrm{d}r u\cdot u\rho\,; \tag{3.24b}$$

$$I_u = \int \mathrm{d}r\kappa[(\nabla_\alpha u_i)^2 - \tfrac{1}{2}u_\alpha\nabla^2 u_\alpha]\,; \tag{3.24c}$$

$$I_v = \tfrac{1}{2}\int \mathrm{d}r\delta\dot{\rho}[(\delta U/\delta\rho)\delta\dot{\rho} - \nabla U_0\cdot u]\,. \tag{3.24d}$$

The integral I_M is the usual classical inertia associated with the displacement field u. The integral I_u is a collective potential energy which derives

from the single-particle kinetic energy. The last integral I_v is a true potential energy.

Our derivation was based on small amplitudes, on irrotational flow, and on the classical Vlasov equation. A similar formula can be derived in the full quantum theory. The starting point is the small-amplitude mean field theory, which is known as RPA. By making an ansatz equivalent to eq. (3.3), a formula is derived from RPA which is the same as eq. (3.24), with an additional integral in the numerator. This additional term has fourth-order derivatives of the field $\boldsymbol{u}$. It is easy to see that such fourth order terms are needed to describe single particle motion correctly in the quantum theory. For if a field $\boldsymbol{u} = \exp(i\boldsymbol{k}\cdot\boldsymbol{r})$ is applied to a particle at rest, the theory should give its energy as $k^2/2m$. The square of the frequency or energy must then be proportional to the fourth derivative of $\boldsymbol{u}$.

Exercise. At what point in the derivation of eq. (3.24) was the capability of describing single particle motion lost?

The full quantum treatment also allows a rigorous physical interpretation for the frequency ω^2 derived above [3.1]. It is a mean frequency associated with the motion described by the field u. The mean is evaluated as the ratio of the expectation of the Hamiltonian to the third power to the expectation of the Hamiltonian in the state made by applying the field $M = \exp(i\phi)$ to the ground state, where

$$\boldsymbol{u} = \boldsymbol{\nabla}\phi\,.$$

Thus

$$\omega^2 = \langle M[H,[H,[H,M]]]\rangle/\langle M[H,M]\rangle\,. \tag{3.25}$$

From this interpretation we see that the formula is a variational principle in the sense that it always gives an upper bound for the frequency of the lowest state. However, the minimum only coincides with an eigenfrequency if the eigenstate is described exactly by applying the field M to the ground state.

As an elementary application of eq. (3.24), we can calculate the quadrupole frequency of the harmonic oscillator. The ground state distribution function for a harmonic oscillator of frequency ω and length parameter

$$v = \omega/m \tag{3.26}$$

is given by

$$f_0 = \exp(-vr^2)\exp(-p^2/v)\,. \tag{3.27}$$

We can take as the quadrupole field the following

$$\boldsymbol{u}_Q = (y, x, 0)\exp(-i\omega t)\,. \tag{3.28}$$

Then the p-odd distribution function from eq. (3.3) is

$$f_u = (2/v)(xp_y + yp_x)f_0\exp(-i\omega t)\,. \tag{3.29}$$

The p-even distribution function from eq. (3.8) satisfies

$$\partial f_g/\partial t = 4[(p_x p_y/v) - vxy]f_0\exp(-i\omega t)\,. \tag{3.30}$$

It can then be verified that eq. (3.17) is satisfied exactly with

$$\omega^2 = 4v^2\,. \tag{3.31}$$

Exercise. Verify eq. (3.31) directly and from eq. (3.24).

We now apply the variational principle to estimate the frequencies of nuclear vibrations of various multipolarity. The estimate will be based on a velocity potential of the form $r^l P^l(\cos\theta)$, so the field to be considered is

$$\boldsymbol{u} = \boldsymbol{\nabla} r^l P^l(\cos\theta)\,. \tag{3.32}$$

The integrals I_M, I_u and I_v can be computed most easily if we use the function $(x + iy)^l$ rather than $r^l P^l(\cos\theta)$. With this function, the field is

$$\boldsymbol{u} = l(\hat{\boldsymbol{x}} + i\hat{\boldsymbol{y}})(x + iy)^{l-1}\,. \tag{3.33}$$

The inertia integral I_M requires the scalar product of $\boldsymbol{u}$ with itself, which is

$$u\cdot u = 2l^2(x^2 + y^2)^{l-1}\,. \tag{3.34}$$

If we use a uniform model for the nuclear density distribution ρ, I_M can be calculated in terms of the number of nucleons A and the radius of the nucleus R. We find

$$\begin{aligned} I_M &= \tfrac{1}{2}\int \mathrm{d}r\rho u\cdot u = l^2\cdot Am\cdot\int_0^R (x^2+y^2)^{l-1}r^2\,\mathrm{d}r\Big/\int_0^R r^2\,\mathrm{d}r \\ &= 3lmA(\tfrac{2}{3})^{l-1}(1/R^3)\int_0^R r^{2l}\,\mathrm{d}r \\ &= 3l^2mA(\tfrac{2}{3})^{l-1}[R^{2l-2}/(2l+1)]\,. \end{aligned} \tag{3.35}$$

To compute I_u, we first need the gradient of the field $\boldsymbol{u}$. This is

$$\nabla_\alpha u_i = l(l-1)(\hat{\boldsymbol{x}} + i\hat{\boldsymbol{y}})_\alpha(\hat{\boldsymbol{x}} + i\hat{\boldsymbol{y}})_i(x + iy)^{l-2}\,. \tag{3.36}$$

The scalar product of this gradient with itself is

$$\sum_{\alpha,i} (\nabla_\alpha u_i)(\nabla_\alpha u_i) = 4l^2(l-1)(x^2+y^2)^{l-2} . \tag{3.37}$$

Only this term contributes to the integral I_u, since the divergence of $\boldsymbol{u}$ vanishes. We find for the integral

$$I_u = \int \mathrm{d}r k(\nabla_\alpha u_i)^2 = \frac{\langle p^2 \rangle}{3m} 4l^2(l-1)^2 \left(\frac{2}{3}\right)^{l-2} \frac{3R^{2l-4}}{2l-1} A . \tag{3.38}$$

The remaining integral involves the interactions. If we assume that the interaction is short range, then

$$u \cdot \nabla U_0 = \frac{\delta U}{\delta \rho} u \cdot \nabla \rho = \frac{\delta U}{\delta \rho} \delta \dot{\rho} . \tag{3.39}$$

The last equality follows from the fact that the divergence of u vanishes. We see from eqs. (3.39) and (3.24d) that the integral I_v vanishes. The total potential energy is unchanged with these coherent disturbances. Finally, substituting eqs. (3.35) and (3.38) in eq. (3.24), we find for the frequency

$$\omega^2 = \frac{(l-1)^2(2l+1)}{5(2l-1)} 6 \frac{p_F^2}{m^2 R^2} . \tag{3.40}$$

Note that the frequency vanishes for $l = 1$. This is as it should be, for the $l = 1$ field is just a uniform translation of the nucleus. Asymptotically, the frequency is proportional to l. In contrast, in the liquid drop model, the frequency is given by

$$\omega^2 = (\sigma / m\rho R^3) L(L-1)(L+2) , \tag{3.41}$$

which has an entirely different dependence on L and R. It is amusing to compare the eqs. (3.40) and (3.41) with each other and with experiment. Reasonable parameters for eq. (3.40) are $p_F = 1.34\ \mathrm{fm}^{-1}$, $1/m = 41.5$ MeV fm, and $R = 1.2\, A^{1/3}$. Then we find for the quadrupole frequency from eq. (3.40)

$$\omega_Q \approx \left(\frac{6 \cdot 5}{5 \cdot 3}\right)^{1/2} \frac{(41.5) \times (1.34)}{(1.2) A^{1/3}} \approx \frac{65}{A^{1/3}} \mathrm{MeV} .$$

Experimentally, the so-called giant quadrupole has an energy of $63/A^{1/3}$ in heavy nuclei. Turning to eq. (3.41), reasonable parameters are $\sigma = 1$ MeV fm^{-2}, $m\rho = 0.16/41.5$ MeV^{-1} fm^{-5}. Then we find for $L = 2$

$$\omega_{L0} = \left(\frac{(41.5) \times 8}{(1.2)^3 (0.16)(A)}\right)^{1/2} = \frac{34}{A^{1/2}} .$$

For $A = 208$, this formula yields an energy of 2 MeV, which is absurdly low.

For monopole vibrations, the interaction will play a crucial role. If we apply the field $\boldsymbol{r}$, which corresponds to a uniform squeezing of the nucleus, we have $\nabla \cdot u = 3$, $\sum_\alpha (\nabla_\alpha u_j)^2 = 3$, and the integrals are

$$I_M = \tfrac{1}{2} m A \cdot \tfrac{3}{5} R^2 , \qquad I_u = 3 \cdot (p_F^2 / 5m) A , \qquad I_v \simeq \tfrac{1}{2} 9 A (\rho [\delta U / \delta \rho]) .$$

In the last integral, we write

$$\delta \dot{\rho} = \nabla \cdot u\rho + u \cdot \nabla \rho$$

and neglect the $u \cdot \nabla$ term in the surface. The result for the monopole frequency is

$$\omega^2 = (9 / m \tfrac{3}{5} R^2)[(2/15)(p_F^2/m) + \rho(\delta U / \delta \rho)] .$$

The expression in square brackets is similar to, but not identical with, the bulk modulus defined as the expression

$$k = (\partial / \partial \rho) \rho^2 (\partial E / A) / \partial \rho$$

evaluated in Hartree–Fock theory. In sect. 4 we will consider specific models and determine the monopole frequencies that are implied. To date, the energy of this mode of motion has not been established experimentally.

Study problem. Generalize the theory of small vibrations to include fields which depend on $\boldsymbol{p}$ as well as $\boldsymbol{r}$. The most important application would be to the $L = 3$ vibration, which should have an eigenmode at an energy much lower than that given by eq. (3.41).

---

4. Bulk properties of nuclear matter

4.1. Equation of state

The properties of finite nuclei tell us only about a single point in the equation of state of nuclear matter. From systematics of nuclear masses and sizes we know that the saturation density is

$$\rho_0 = 0.17\ \text{nucleons/fm}^3$$

and the binding energy at saturation is 16 MeV/particle, if the Coulomb force is dropped. All other information on the equation of state is inference from theoretical calculations or by analogy to other systems. Unfortunately, the theory is not in as good shape as might be hoped: the best

calculations in the Brueckner theory predict either substantially higher densities or substantially weaker binding than the empirical. So the best theory can do at the moment is to provide a functional form for the equation of state. By fitting parameters to the ground state properties, it might be hoped that a prediction for other densities would be obtained. The simplest model one could consider is a dilute gas of particles interacting by a short range repulsive potential. Since the gas is dilute, the only property of the interaction that is significant is the scattering length a. It is then possible to expand the ground state energy in powers of a, as follows:

$$\frac{E}{A} = \frac{p_F^2}{2m}\left[\frac{3}{5} + \frac{2}{\pi}p_F a + \frac{12}{35\pi^2}(11 - 2\ln 2)(p_F a)^2 + 0.78(p_F a)^3 + \cdots\right]. \tag{4.1}$$

The first term is just the kinetic energy of a free Fermi gas. The second term is the first order interaction between the particles. It behaves as though the particles interacted in Born approximation via a short-range potential. This potential is given by the phase shift approximation,

$$v(k) = (4\pi/mk)\delta_0 = (4\pi/m)a\,, \tag{4.2}$$

where δ_0 is the s-wave phase shift for pairs of momentum k. The matrix element of the above potential, evaluated in a determinantal wavefunction, gives the second term in eq. (4.1). In a many-body wavefunction the pair correlations cannot be optimal to minimize the two-body energy, because of the Pauli principle. This effect is contained in the third term in the series eq. (4.1), a repulsive correction first found by Huang and Yang [4.1]. An additional term has been computed [4.2] in this expansion in orders of $(p_F a)$, and is given in eq. (4.1). To make use of this power series to construct an equation of state, the first term can be taken as is. Since the saturation binding and density provide two pieces of information, the equation of state could be parameterized using the next two terms in the series. In terms of density instead of p_F, this would be

$$E/A = \langle T\rangle(\rho/\rho_0)^{2/3} + a(\rho/\rho_0) + b(\rho/\rho_0)^{4/3}\,, \tag{4.3}$$

with $\langle T\rangle = 23$ MeV, and a and b now parameters to be fixed. However, a dilute gas may not be the best model since its saturation properties are not evident. If one assumes that the saturation is due to a momentum dependence in the effective interaction, a different parameterization emerges. The interaction would depend on p as

$$v = v(r_{12}) + (p_1 - p_2)^2 v'(r_{12})\,. \tag{4.4}$$

Taking the expectation of this potential in the free Fermi gas, we find that the second term is proportional to $\rho\langle p^2\rangle \sim \rho^{5/3}$. Thus the parameterization with three terms would be

$$E/A = \langle T\rangle(\rho/\rho_0)^{2/3} + a(\rho/\rho_0) + b(\rho/\rho_0)^{5/3}\,. \tag{4.5}$$

This form is used by Myers and Swiatecki [4.3]. Finally, the saturation could be mostly due to the so-called dispersion correction to the tensor interaction. This is an effect that seems to depend on three-particle spatial correlations rather than the Pauli principle and thus has a quadratic dependence on density. The equation of state in this model would be parameterized by

$$E/A = \langle T\rangle(\rho/\rho_0)^{2/3} + a(\rho/\rho_0) + b(\rho/\rho_0)^2\,. \tag{4.6}$$

A model of the nuclear many-body system which was revived by Vautherin and Brink [4.4] is based on a very simplified parameterization of the interaction introduced by Skyrme. This interaction has zero range, but includes possible momentum dependence and density dependence. The Hamiltonian is only calculated in the Hartree–Fock approximation. This scheme provides a range of models for the equation of state which includes both eq. (4.5) and (4.6).

For each of these models, the coefficients a and b can be determined from the conditions

$$(E/A)|_{\rho_0} = -E_B = -16\ \text{MeV} \quad \text{binding energy} \tag{4.7}$$

$$P = -\frac{\partial E/A}{\partial v/A} = \rho_2 \frac{\partial E/A}{\partial \rho}\bigg|_{\rho_0} \quad \text{saturation} \tag{4.8}$$

Zamick [4.5] has discussed the equation of state obtained as a function of the exponent in the last term in the expansion, which he writes as $(\sigma + 1)$. From eqs. (4.7) and (4.8) the equations are obtained

$$-E_B = \langle T\rangle + a + b\,, \qquad 0 = \tfrac{2}{3}\langle T\rangle + a + (\sigma + 1)b\,. \tag{4.9}$$

These can be solved to give

$$a = -\frac{\sigma + 1}{\sigma}E_B - \langle T\rangle\frac{\sigma + \frac{1}{3}}{\sigma}\,, \qquad b = \frac{E_B}{\sigma} + \tfrac{1}{3}\frac{\langle T\rangle}{\sigma}\,.$$

Two properties of the resulting equation of state are of special interest: the compressibility and the energy per particle at twice normal density. If compressibility is defined in the conventional way,

$$k = v(\partial P/\partial v)\,,$$

then Zamick finds

$$k = \rho_0[\tfrac{1}{9}\langle T\rangle + E_B + \sigma(\tfrac{1}{3}\langle T\rangle + E_B)] . \quad (4.10)$$

Note: there is a convention in nuclear physics, which will not be followed here, to define a compressibility as $K = 9k/\rho_0$.

Exercise. Verify eq. (4.10).

Once the compressibility is known, the thermal sound velocity is given by

$$c_t = (k/m\rho_0)^{1/2} \quad (4.11)$$

and the longitudinal sound velocity is given by

$$c_l = [(k + \tfrac{4}{3}\mu)/m\rho_0]^{1/2} , \quad (4.12)$$

where

$$\mu = p_F^2\rho_0/5m .$$

Applying eq. (4.10) to the various candidate equations of state, we find the following possible compressibilities and sound velocities:

	$\sigma = \frac{1}{3}$	$\sigma = \frac{2}{3}$	$\sigma = 1$
k/ρ_0 (MeV)	26.4	34.3	42
c_t	$0.17c$	$0.19c$	$0.21c$
c_l	$0.22c$	$0.24c$	$0.26c$

In all cases these velocities are below the Fermi velocity, $v_F \approx 0.28c$. From this it seems likely that nuclear matter does not support the undamped waves of Landau theory. Before insisting on that conclusion too strongly, it is well to examine the behavior of the only other Fermi liquid with short-range interactions, liquid ^{3}He. For this system, the binding energy is 2.14×10^{-4} eV and the kinetic energy of the free Fermi gas is 2.63×10^{-4} eV. As in the nuclear case, the kinetic energy is slightly larger than the binding energy. The compressibility according to eq. (4.10) would be

$$k/\rho_0 = 5.5 \times 10^{-4}\,\text{eV} , \qquad (\sigma = 1) .$$

In fact the coefficient is actually nearly a factor of two larger. Thus our simple models do not work in the ^{3}He system.

Exercise. Determine the empirical compressibility of ^{3}He, using the empirical sound velocity

$$c_t = 183\ \text{ms}^{-1}$$

The lesson is that we should not place too much reliance on models for the nuclear system, but wait until more evidence is available. The best evidence would be observation of the giant monopole state in medium-weight or heavy nuclei. The energy of this state is proportional to the square root of the compressibility, as was seen in sect. 3.

The sound velocity should always be lower than the velocity of light, if a basic precept of relativity is not to be violated. This provides a constraint on the compressibility, since eq. (4.11) is valid relativistically. When the density becomes high, the highest power in the equation of state governs the compressibility: we find with the model equations of state

$$c_t \to (\sigma + 1)c . \quad (4.13)$$

Thus we must have $\sigma = 0$ asymptotically. Relativistic equations of state can be derived to satisfy this. The short range repulsion is provided by a vector meson. It is possible to formulate a relativistic [4.6] Hartree–Fock model that is asymptotically correct, and that binds nuclear matter correctly. There are two parameters, the strength of the vector meson and the strength of a scalar meson. The vector meson field is always repulsive, but the scalar field is attractive at low density. The compressibility in this model comes out to $k/\rho_0 = 60$ MeV, which is substantially higher than the other models.

Problem. What is the maximum density in a relativistic shock wave?

Another interesting quantity obtainable from the equation of state is the energy per particle at twice normal density. A density of twice normal should be achievable without much difficulty by heavy ion collisions at sufficiently high energy. Providing the degree of overlap of the nuclei in a heavy ion collision had some experimental signature, the energy required to achieve this overlap would be a useful indicator of the stiffness of the equation of state. One of the main theoretical problems of heavy ion theory is to find such an experimental signature.

Exercise. Determine the energy at $2\rho_0$ for the various equations of state.

The result is that there is about zero energy per particle at $2\rho_0$. Since the initial energy was -16 MeV, the projectile must bring in 16 MeV/particle in the center of mass frame. In the laboratory frame, the projectile has to bring in twice this energy. Since the number of particles in the system of

overlapping nuclei is twice the number in the projectile, the result is that the bombarding energy of the projectile must be 64 MeV/A. Of course, the actual dynamics would require a much higher bombarding energy, since the nuclear matter at twice normal density would have extra kinetic energy. We will consider this in more detail in the next section.

4.2. Tensile strength of nuclear matter

The equation of state can be used to estimate the tensile strength of nuclear matter. This is the maximum negative pressure that the medium can sustain before snapping. This quantity has relevance both to fission and to strongly damped collisions. The stronger the nuclear medium, the more it can stretch before snapping, and therefore the lower will be the Coulomb energy of the separating fragments. There are several ways we could make this estimate. The first is to use the nuclear matter equation of state, and solve for the maximum negative pressure. The pressure is related to the energy per particle by

$$P = \rho^2(\partial E/A)/\partial\rho\,, \tag{4.14}$$

so the condition that the pressure be a minimum is

$$\frac{\partial P}{\partial\rho} = \frac{\partial}{\partial\rho}\rho^2\frac{\partial E/A}{\partial\rho} = 0$$

$$= \tfrac{2}{3}\cdot\tfrac{5}{3}\langle T\rangle\left(\frac{\rho}{\rho_0}\right)^{2/3} + 2a\left(\frac{\rho}{\rho_0}\right) + (\sigma+1)(\sigma+2)\left(\frac{\rho}{\rho_0}\right)^{5/3}. \tag{4.15}$$

For the $\sigma = 1$ equation of state, the critical density is

$$\rho_{\text{critical}} = 0.62\rho_0 \tag{4.16}$$

and the pressure is

$$P = -0.7\ \text{MeV fm}^{-3}\,. \tag{4.17}$$

If this pressure is exceeded, the nuclear matter will become unstable against long-wavelength density fluctuations. The density fluctuation will increase in amplitude until the medium is separated into regions of zero density and regions of normal density.

In discussing the fission of nuclei the surface energy also plays a role in preventing the nucleus from stretching. The total force between the two halves of the nucleus is given by a sum of two terms,

$$F = \sigma C + PA\,, \tag{4.18}$$

where σ is the surface energy, C is the circumference of the neck region, and A is the area of the neck region. Under normal nuclear matter conditions

$$\sigma \approx 1\ \text{MeV fm}^{-2}\,. \tag{4.19}$$

For a neck radius of 2 fm, the force is

$$F = 12.6\ \text{MeV fm}^{-2}|_{\text{surface}} + 8.8\ \text{MeV fm}^{-2}|_{\text{volume}}\,. \tag{4.20}$$

Thus the internal negative pressure will make a contribution of about the same order of magnitude as the surface energy. The tensile strength can also be studied in the time-dependent Hartree–Fock theory. This should give the same results as the above calculation, because the condition for a pressure extremum, eq. (4.15), is equivalent to a long wavelength instability in RPA, the small amplitude time-dependent Hartree–Fock theory. An example of a time-dependent Hartree–Fock calculation is shown in fig. 10. This is a calculation of fission of ^{236}U by Negele. The shape of the U nucleus is shown at different times, starting from the saddle point. The dashed line is a contour of $\rho = \rho_0$, and the middle solid line is a contour of $\rho = \frac{1}{2}\rho_0$. In order to allow the system to fission the particles must be allowed to change orbits, so that the Fermi surface remains approximately spherical. Of course this feature of changing orbits is not in TDHF, and had to be included ad hoc. The results are that the system creeps out in shape as the particles are shifting orbits. Just after the next to last picture, the neck snaps with no further orbit shifting needed. The neck radius, measured at half-density contour, is 1.5 fm. The density is well above the estimate from eq. (4.16) when scission occurs. Of course in eq. (4.16) we have assumed infinite matter: in the TDHF calculation the neck is practically all surface. Perhaps this explains the discrepancy.

Study problem. How does the tensile strength depend on the functional form of the equation of state? Is nuclear matter stronger for a stiff equation of state or for a soft equation of state?

Problem. Determine the heaviest projectile that can fuse with ^{208}Pb, assuming that the fused system has a configuration of two intersecting spheres, and that the Coulomb force does not exceed the tensile strength of the interface.

Another approach to the tensile strength of nuclear matter is to consider the inverse question, of how much force the two separated fragments exert on each other. Let us imagine that we bring together two slabs of nuclear matter. When the surfaces just touch, the surface energy of the

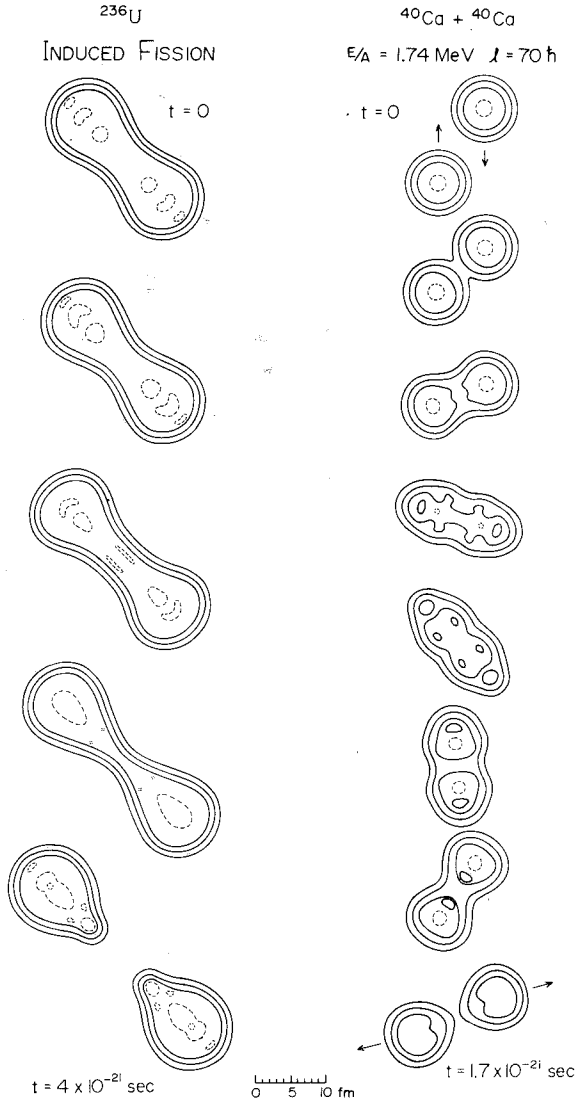

Fig. 10. Fission of ^{236}U in time dependent Hartree–Fock theory.

individual slabs will roughly disappear. So, if we know the functional form of the interaction between the surfaces, we can get the magnitude by demanding that the energy difference per unit area satisfies

$$E(\infty) - E(\sigma) = 2\sigma\,. \tag{4.21}$$

The functional form of the interaction can be fixed by assuming some model potential. Randrup determines the interaction in this way to be [4.7]

$$\begin{aligned} E &= -2(0.9263 + 0.1790x - 0.4355x^2 + 0.0889x^3) && x < 2 \\ &= -2(6.168)\exp(-x/0.65)\,, && x > 2 \end{aligned} \tag{4.22}$$

where x is the distance between the surfaces in fm. The force per unit area is the derivative of eq. (4.22), which is

$$\begin{aligned} P &= -2(0.1790 - 0.871x + 0.2667x^2) && x < 2 \\ &= -2(9.858)\exp(-x/0.65)\,. \end{aligned} \tag{4.23}$$

The maximum this force can be is ~ 1 MeV fm^{-3}, which is close to the tensile strength eq. (4.17). There is no reason for these numbers to be the same. First, the derivation of the force of attraction between the nuclei just considered the static interactions between densities of two slabs, taking no account of the Pauli principle. However, phenomenological support can be given to the interaction by the elastic scattering of heavy ions. So we need not worry too much about this point. But also the force pulling two nuclei together can only be the same as the force required to pull them apart if there is no internal energy created in the process. The near equality of the force of attraction with the tensile strength suggests that if the classical fusion barrier is surmounted in a collision, the nuclei will remain fused until longer time scale shape changes can take place. This view is supported by the light ion data, which requires only consideration of a fusion barrier in the entrance channel.

5. Dissipation of collective motion

In the present section we study the dissipation of coherent motion in finite systems. Our starting point is the Vlasov equation, including a collision term,

$$(\partial f/\partial t) + v\cdot\nabla f - \nabla U\cdot\nabla^p f = I\,. \tag{5.1}$$

Suppose the system is initially in its ground state, and is perturbed slightly from equilibrium. The system will then oscillate about the equilibrium,

and in general the evolution of some simple observable, such as the current, will be a decaying oscillating function. The dissipation may be characterized by the decay envelope of the oscillation. The exact definition will of course depend on which observables are considered.

There are two quite distinct mechanisms of dissipation. If dissipation comes about through terms on the left-hand side of eq. (5.1), it is built into the one-body theory. This would be called Landau damping in the theory of infinite systems. The right-hand side of eq. (5.1) is the change in distribution function due to two-body collisions. In certain situations, this two-body dissipation term will dominate.

5.1. Landau damping

Let us first neglect the collision term and see under what conditions dissipation is present in the Vlasov equation. Consider a distribution which is perturbed from the ground state by imposing a velocity field $\boldsymbol{u}$ on the ground state distribution function. This is

$$f = f_0 - \boldsymbol{u}\cdot\nabla^p f_0 \,. \tag{5.2}$$

This is substituted in the Vlasov equation, as was done in obtaining eq. (3.13). Confining our attention to the interior of the nucleus, where $U_0 = 0$ and $\nabla_x f_0 = 0$, eq. (3.13) becomes

$$u\cdot\nabla^p f_0 + v\cdot\nabla v\cdot\nabla u\cdot\nabla^p f_0 - \nabla[(\delta U/\delta\rho)\delta\rho]\cdot\nabla^p f_0 = 0 \,. \tag{5.3}$$

In general it is not possible for a sinusoidal $\boldsymbol{u}(r)$ to satisfy this equation since the second term introduces a v dependence. However, if $\delta U/\delta\rho$ is large and repulsive, the middle term will be unimportant and a single collective state will dominate the response. This is the condition for the zero sound collective mode of the Landau theory. In the situation where the third term is not dominant, the damping time will be determined by the second term. For different angles in momentum space, the second term ranges in size from zero to

$$({}^vF/\lambda)^2\cdot u\cdot\nabla^p f_0$$

where λ is the wavelength of the disturbance,

$$\nabla u \sim u/\lambda \,.$$

Thus the coherent field u will spread out into eigenmodes having frequencies ranging from zero to ${}^vF/\lambda$.

This damping, called Landau damping, follows from the fact that the particles carrying the disturbance travel at different velocities, causing eventual incoherence. The time scale for Landau damping is different from that of viscocity, which has a damping time of order

$$t = \rho\lambda^2/\eta \tag{5.4}$$

where η is the coefficient of viscosity.

There is an exception to the rule that an attractive $\delta U/\delta\rho$ implies Landau damping. Namely, if the field $\boldsymbol{u}$ is linear in r, then the middle term will vanish when the second derivation is taken. Thus, a quadrupole or monopole velocity potential will give rise to a collective motion that is not subject to Landau damping. Physically, the reason for the stability of these modes is that the distortion of the Fermi surface is uniform throughout the nucleus. Then the independent propagation of the particles does not lead to a change in the shape of the Fermi surface. That this is truly a classical and not a quantum phenomenon has been seen by numerical experiment on classical particles in boxes with vibrating walls. In this classical model there are no collisions between the particles, but the energy and momentum of the particles can change when the particles collide with the moving wall. If the box vibration has a high multipolarity, the wall motion quickly transfers incoherent energy to the particles in the box. If the vibration is monopole, dipole, or quadrupole, the particles do not get heated up, but coherently exchange energy with the box.

5.2. Two-body dissipation

We have so far neglected the collision term on the right-hand side of eq. (5.1). The effect of two-body collisions on the one-particle density can be calculated analytically in two limits: (a) a single particle outside a Fermi sphere, interacting with a short-range potential, (b) a single particle in a finite temperature distribution. The first case was calculated by Galitskii [5.1] with the result

$$1/\tau = \langle\sigma\rho\rangle v_{\mathrm{F}}\tfrac{3}{4}(\varepsilon_{\mathrm{F}} - \varepsilon)^2/\varepsilon_{\mathrm{F}} \tag{5.5}$$

where σ is nucleon–nucleon cross-section, ρ is the density, ε_{F} is the Fermi energy, and ε is the energy of the particle travelling through the nuclear medium.

This formula will now be derived, following Kikuchi and Kawai [5.2]. A collision is considered between the external particle, having momentum p_1, and a particle in the Fermi sea which has momentum p_2. After the

collision the two particles end up with momenta p_1' and p_2'. The Pauli principle requires that both these momenta lie above the Fermi level, p_F. Calling the relative momentum of the two particles

$$p = \tfrac{1}{2}(p_1 - p_2)\,,$$

the sum over final states includes an integral over $\hat{p}$, restricted by:

$$p^2 + \tfrac{1}{4}p_{cm}^2 \pm pp_{cm}\cos\hat{p} = p_F^2\,. \tag{5.6}$$

The effective cross-section for scattering, taking account of the exclusion principle, is then

$$\sigma_{eff} = \frac{1}{p_1}\int^{p_F} p_2^2\,dp_2 \int d\hat{p}_2 \int d\Omega\,\frac{2p\,d\sigma(p)}{d\Omega} \Big/ \int^{p_F} d^3p_2\,. \tag{5.7}$$

The angular integration over $\hat{p}$ for the final states yields

$$d\Omega\,d\sigma/d\Omega = \sigma\cos\hat{p} = \sigma(p^2 + \tfrac{1}{4}p_{cm}^2 - p_F^2)/pp_{cm}\,. \tag{5.8}$$

The numerator can be rewritten

$$\tfrac{1}{4}(\boldsymbol{p}_1 - \boldsymbol{p}_2)^2 + \tfrac{1}{4}(\boldsymbol{p}_1 + \boldsymbol{p}_2)^2 - p_F^2 = \tfrac{1}{2}p_1^2 + \tfrac{1}{2}p_2^2 - p_F^2\,. \tag{5.9}$$

Then the integral over $d\hat{p}_2$ becomes

$$2\pi\int 2p\sigma\,\frac{(p_1^2 + p_2^2 - 2p_F^2)\,d\hat{p}_1\cdot\hat{p}_2}{2p(p_1^2 + p_2^2 - 2\hat{p}_1\cdot\hat{p}_2 p_1 p_2)^{1/2}} = 2\pi\sigma(p_1^2 + p_2^2 - 2p_F)\frac{2}{p_1}\,. \tag{5.10}$$

There is one remaining integral over dp_2 to determine the effective cross-section. The lower limit of this integral is fixed by the position where $\int d\Omega$ vanishes,

$$\sigma_{eff} = \frac{4\pi\sigma}{p_1^2}\int_{(2p_F^2 - p_1^2)^{1/2}}^{p_F} (p_1^2 + p_2^2 - 2p_F^2)p_2^2\,dp_2 \Big/ \int_0^{p_F} d^3p_2\,. \tag{5.11}$$

The result is

$$\sigma_{eff} = \sigma\left[1 - \frac{7}{5}\left(\frac{p_F}{p_1}\right)^2 + \frac{2}{5p_F^3p_1^2}(2p_F^2 - p_1^2)^{5/2}\right]. \tag{5.12}$$

This may be expanded in powers of

$$\Delta\varepsilon/\varepsilon_F = (p_1^2 - p_F^2)/p_F^2\,. \tag{5.13}$$

The lowest non-vanishing power is quadratic and is given by

$$\sigma_{eff} = \tfrac{3}{4}\bar{\sigma}(\Delta\varepsilon/\varepsilon_F)^2\,. \tag{5.14}$$

To use this formula we need an estimate of the mean cross-section. For free nucleons, in the energy range 35–300 MeV the cross-section is well described by the formula [5.3],

$$\bar{\sigma} = \tfrac{1}{2}(\sigma_{pp} + \sigma_{np}) = (62.5 - 56.06/\beta + 22.36/\beta^2)\,\text{mb}\,, \tag{5.15}$$

where β is the velocity of the incoming nucleon in units of the velocity of light. For example, a nucleon travelling with the Fermi velocity has a velocity of $\beta = 0.28$, and the cross-section of nucleons at rest is 145 mb according to the formula, compared with 145 mb from compilations [5.4, 5.5] of the measured cross-sections. When this data is combined with the Fermi gas theory, one finds an effective cross-section which is small at low energies, varying approximately as

$$\sigma_{eff} \approx 150\,\text{mb}(\Delta\varepsilon/\varepsilon_F)^2\,, \tag{5.16}$$

and increasing to about 20 mb for energies in the range 100 MeV–400 MeV. The mean free path of nucleons is related to this cross effective cross-section by

$$\lambda = 1/\sigma_{eff}\rho\,. \tag{5.17}$$

The mean free path computed this way varies from 7 fm at energy 10 MeV above the Fermi level, decreasing to a plateau of about 2.6 fm at higher energies. Due to the fact that the nuclear cross-sections are forward peaked, the Pauli exclusion is important at even the highest energies.

The approximation of using the free nucleon cross-sections is unreliable at low relative momentum. When the momentum is low, the free cross-section is dominated by the large S-wave phase shifts, and so the momentum sets the scale for the collisions. In the nuclear medium, these extremely long range correlations are inhibited by the Pauli principle. The proper procedure is to solve the scattering problem with the excluded phase space explicitly taken into account. This has been done by Mahaux and collaborators [5.6]. They also include the effect of the medium on the density of states. They find an effective cross-section of about 120 mb for low energy particles.

The most reliable information on nucleon mean free paths comes from the optical model. Nuclei are known to be somewhat transparent to nucleons, from the variations of the total cross-section with the energy of the projectile and mass number of the target nucleus [5.7]. The semi-classical mean free path is related to the imaginary optical potential by

$$\lambda = 1/2\,\text{Im}\,k = 1/2\,\text{Im}[(E + V + iW)2m]^{1/2}\,, \tag{5.18}$$

where V is the real part of the potential in the nucleus, W is the imaginary potential, and E is the kinetic energy of the nucleon just outside the nucleus.

Unfortunately, much of the absorption takes place at the nuclear surface, and it is not possible to distinguish this experimentally. However, the data can be fit assuming W constant in the nuclear interior. One such potential, determined from the elastic scattering of 156 MeV protons on ^{208}Pb is [5.8]:

$$E = 140 \text{ MeV} ; \qquad V = 17 \text{ MeV} ; \qquad W = 12 \text{ MeV} .$$

These numbers, when inserted in eq. (5.18), yield $\lambda = 4.8$ fm. The Fermi gas calculation, based on the free nucleon–nucleon cross-section, gives smaller mean free path by a factor of two. The mean free path computed in ref. [5.6] is much closer, but also too small.

The mean free path decreases when there are excitations already present in the medium, because the available phase space for scattering increases. It is possible to generalize eq. (5.14) to Fermi gases at finite temperature. Denoting the temperature of the Fermi gas by T, the result is [5.9]

$$\sigma_{\text{eff}} = \tfrac{3}{4}\bar{\sigma}[(\Delta\varepsilon)^2 + (\pi T)^2]/\varepsilon_{\text{F}}^2[1 + \exp(-\Delta\varepsilon/T)] \tag{5.19}$$

Thus for energies less than πT, the collision cross-section is dominated by the scattering from excitations of the system. A typical temperature is 2 MeV, in which case the mean free path of a particle at the Fermi surface would be

$$\lambda = 1/\sigma_{\text{eff}}\rho = [\tfrac{3}{4}(145)(\pi\cdot 2)^2(0.16)/(37)^2\cdot 2]^{-1} = 40 \text{ fm} . \tag{5.20}$$

5.3. *Viscosity*

Knowing the collision rate at finite temperature, it is possible to calculate the ordinary hydrodynamic viscosity of an infinite Fermi liquid [5.10]. The resulting expression will not be of immediate use, since as was seen in eq. (5.20) the length scale for the collisions is larger than the size of the nuclei. However, viscosity has been used as a phenomenological parameter in discussing nuclear dissipation. Also, the calculational technique will have other applications. The viscosity coefficient is defined as the momentum transported across a unit area per unit time, for a unit velocity gradient in the perpendicular direction. Two coefficients of viscosity can be defined, depending on whether the velocity field is parallel or perpendicular to the gradient. The more interesting case is the usual one with the velocity perpendicular to the gradient. To determine the viscosity, it is first necessary to find the distribution function for the assumed flow field. Suppose the velocity field is given by

$$\boldsymbol{v} = (\mathrm{d}v/\mathrm{d}x)xz .$$

Then the distribution function in the vicinity of $x = 0$ will have the form

$$f = f_0 - mx\,\mathrm{d}v/\mathrm{d}x\;\nabla_z^p f_0 + f_g , \tag{5.21}$$

where f_g is small. This distribution is assumed to be independent of time. Then f_g may be determined from the Boltzmann equation,

$$v\cdot\nabla f = I(f) . \tag{5.22}$$

The collision integral depends on the distribution function as follows

$$\begin{aligned} I_{p_1} = \int \mathrm{d}\boldsymbol{p}_2\,\mathrm{d}\boldsymbol{p}_3\,\mathrm{d}\boldsymbol{p}_4\{&f(p_3)f(p_4)[1-\tilde{f}(p_1)][1-\tilde{f}(p_2)] - f(p_1)f(p_2)\\ &\times[1-\tilde{f}(p_3)](1-\tilde{f}(p_4)\}\delta(p_1+p_2-p_3-p_4)\\ &\times\delta(E_1+E_2-E_3-E_4)8\pi^2\sigma/m^2 , \qquad \text{where } \tilde{f} = f/(2\pi)^3 . \end{aligned} \tag{5.23}$$

The second term in eq. (5.21) makes no contribution to the collision integral since the collisions must conserve current. So the equation to be satisfied is

$$-v\cdot\nabla m \times (\mathrm{d}v/\mathrm{d}x)\nabla_z^p f_0 = -\,m(\mathrm{d}v/\mathrm{d}x)v_x\nabla_z^p f_0 = I(f_g) . \tag{5.24}$$

This is an integral equation for f_g, and it cannot be solved exactly. In ref. [5.1] a specific functional form is assumed for f_g, and eq. (5.24) is solved at the Fermi level. The obvious functional form to assume is the same form as the left-hand side of eq. (5.24). We write this as

$$f_g = sQ_\lambda^2(\hat{p})\partial f_0/\partial p = sQ_\lambda^2(\hat{p})(1-f_0)f_0 v/T , \tag{5.25}$$

where s is a constant to be determined, Q_λ^2 is a quadrupole function of angle $\hat{p}$, and T is temperature. Then the collision integral may be expanded to first order in s as

$$\begin{aligned} I_{p_1} = \int \mathrm{d}\boldsymbol{p}_2\,\mathrm{d}\boldsymbol{p}_3\,\mathrm{d}\boldsymbol{p}_4 &f_0(p_1)f_0(p_2)[1-\tilde{f}_0(p_3)][1-\tilde{f}_0(p_4)]\\ &\times[Q_\lambda^2(\hat{p}_1)+Q_\lambda^2(\hat{p}_2)-Q^2(\hat{p}_3)-Q_\lambda^2(\hat{p}_4)]\delta(p_1+p_2-p_3-p_4)\\ &\times\delta(E_1+E_2-E_3-E_4)8\pi^2 v s\sigma/m^2T . \end{aligned} \tag{5.26}$$

The addition theorem for spherical harmonics allows a factor of $Q^2(\hat{p}_1)$ to be factored out of the integral, yielding

$$\begin{aligned} I_{p_1} = sQ_\lambda^2(p_1)\int \mathrm{d}\boldsymbol{p}_2\,\mathrm{d}\boldsymbol{p}_3\,\mathrm{d}\boldsymbol{p}_4 &f_0^2(1-f_0)^2\\ &\times[1+P_2(\hat{p}_{12})-P_2(\hat{p}_{13})-P_2(\hat{p}_{14})]\delta^3(p_1+p_2-p_3-p_4)\\ &\times\delta(E_1+E_2-E_3-E_4)8\pi^2 v\sigma/m^2T . \end{aligned} \tag{5.27}$$

This integral is evaluated in the following coordinate system. Denote the angular coordinates of p_2 with respect to p_1 by (θ, ϕ_2), and the angle between the $p_1 - p_2$ plane and the $p_3 - p_4$ plane by ϕ. Also, let x and y be the energies of particles 3 and 4 above the Fermi level. Then the integral may be transformed to

$$\int \mathrm{d}\boldsymbol{p}_2\, \mathrm{d}\boldsymbol{p}_3\, \mathrm{d}\boldsymbol{p}_4 \delta(p)\delta(E) = \tfrac{1}{2}m^3 \int [\mathrm{d}\cos\theta\, \mathrm{d}\phi\, \mathrm{d}\phi_2/\cos\tfrac{1}{2}\theta]\, \mathrm{d}x\, \mathrm{d}y\,. \quad (5.28)$$

The remaining algebra to evaluate this integral is not very interesting. The result can be expressed in terms of a mean life $\tau_{(2)}$ for small quadrupolar distortion of the Fermi sea

$$I(f_g) = f_g/\tau_{(2)}\,. \quad (5.29)$$

Like the single-particle lifetime, $\tau_{(2)}$ varies with temperature as T^{-2}. The distribution function is now given by

$$f = f_0 - m_x(\mathrm{d}v/\mathrm{d}x)\nabla_z^p f_0 - m\tau_{(2)}(\mathrm{d}v/\mathrm{d}x)v_x\nabla_z^p f_0\,.$$

The momentum flux across the xy plane is evaluated as

$$\mathrm{d}P/\mathrm{d}A = \int \mathrm{d}\boldsymbol{p}\, p x v_z f = \tau_{(2)}(\mathrm{d}v/\mathrm{d}x)\langle p_x^2\rangle \rho m \approx \tau_{(2)}(\mathrm{d}v/\mathrm{d}x)\tfrac{1}{3}\langle p^2\rangle \rho m\,. \quad (5.30)$$

The coefficient of $\mathrm{d}v/\mathrm{d}x$ in the last expression is identical to the viscosity of a dilute classical gas, if τ is the mean time for particles to equilibrate momentum by collisions. Thus the only quantum aspect of the physics is the long collision times in a degenerate Fermi system.

Exercise. Assuming a temperature of 1 MeV and $\tau_{(2)} = \tau$ (single-particle), determine the viscosity of nuclear matter.

5.4. *Collisions on deformed Fermi surfaces*

The dissipation in the case of zero temperature comes from collisions which are allowed in a Fermi sea that is distorted from a spherical shape, but still has sharp edges. The lecturer does not know how to calculate the collision rate analytically. But at least we can evaluate the dependence of the collision rate on the magnitude of the distortion. Consider the following parameterization of the Fermi surface,

$$p_F = p_0[1 + \tfrac{1}{2}\alpha P_2(\cos\theta)]\,. \quad (5.31)$$

We wish to determine the rate at which a particle below the Fermi surface makes collisions. We thus have the integral,

$$I_\rho = \int \mathrm{d}\boldsymbol{p}_2\, \mathrm{d}\boldsymbol{p}_3\, \mathrm{d}\boldsymbol{p}_4 \theta[\alpha P_2(\cos\theta_2) - z]\theta[x - \alpha P_2(\cos\theta_3)] \times \theta[y - \alpha P_2(\cos\theta_4)]\delta^3(p)\delta[(t + z - x - y)\varepsilon_F]2\sigma/(2\pi)^2 m^4\,. \quad (5.32)$$

where t, z, x, and y are the respective energies of particles 1, 2, 3, and 4 above the (spherical) Fermi level, expressed in units of the Fermi energy. We make the coordinate transformation eq. (5.28) and consider only the energy integrals which are over x and y. The θ function for z can be replaced by limiting the y integral to $y \leqslant \alpha P_2(\cos\theta_2) - x + t$. The lower limit of this integral is $\alpha P_2(\cos\theta_4)$, due to another θ function. So the y integral can be evaluated as

$$\int_{\alpha P_2(\cos\theta_4)}^{\alpha P_2(\cos\theta_1)+t-x} \mathrm{d}y = \alpha[P_2(\cos\theta_2) - P_2(\cos\theta_4)] + t - x \quad \text{or zero, whichever is greater}\,. \quad (5.33)$$

We can assume that t is proportional to α, taking a representative particle for p_1. Then the x integral can be expressed

$$\int_{\alpha P_2(\cos\theta_3)}^{\alpha[P_2(\cos\theta_2)-P_2(\cos\theta_4)+t_0]} \{\alpha[P_2(\cos\theta_2) - P_2(\cos\theta_4)] + \alpha t_0 - x\}\,. \quad (5.34)$$

This integral is obviously proportional to α^2. Thus the collision rate for particles in this geometry scales the same way with energy as for a single particle outside a spherical Fermi surface.

Study problem. Work out analytically the collision rate for the distorted Fermi sphere.

The lecturer has evaluated the integral (5.26) numerically for a distortion function composed of two spheres which are possibly intersecting. This geometry is shown in fig. 11. The centers of the spheres are separated by a momentum P. The collision rate in this configuration is then only a fraction of the collision rate for a single nucleon located a distance P above the Fermi level. The results of the computer calculation for this rate are given in table 5.1 below.

Table 5.1

P/p_F	0.1	0.5	1.0
I/I_{nucleon}	0.3	0.3	0.6

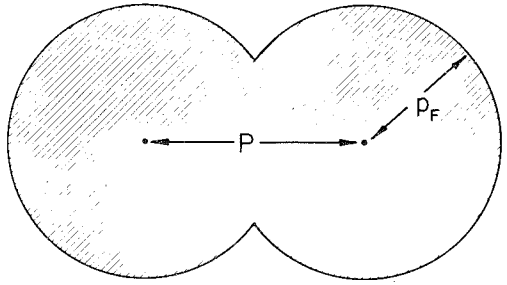

Fig. 11. Distorted Fermi sphere.

Experimental evidence on the dissipation of collective energy is available from the widths of giant resonant states. The best known resonance, the giant dipole, is not appropriate for our purposes because the neutron Fermi surface does not move with the proton Fermi surface. The giant quadrupole state has neutrons and protons moving together, and in the classical model is described by a Fermi surface which undergoes uniform quadrupole oscillations. Empirically the width of the giant quadrupole varies from $\geqslant 10$ MeV in light nuclei to ~ 3 MeV in ^{208}Pb. In the conventional shell model picture this state is a particle–hole state, and its width can be computed from the collisions of the particle and the hole. If the particle and the hole acted independently, the damping rate could be estimated from the single particle rate as

$$\Gamma_{\mathrm{ph}} = (1/E)\int_0^E \mathrm{d}\varepsilon[\Gamma_{\mathrm{p}}(\varepsilon) + \Gamma_{\mathrm{n}}(E-\varepsilon)]$$

where E is the excitation energy of the state. Thus for ^{208}Pb, a particle–hole state at 11 MeV should have a width of about $\frac{2}{3} \times 8 = 5$ MeV. In fact there is a coherence between particle and hole which reduces the collision rate. This coherence is easy to see in the infinite system, and is illustrated in fig. 12 below.

Two possible initial configurations in the collective 1p–1h state can lead to the same 2p–2h state as a result of the collisions. In the figure, a collision of either the particle or the hole can give the final state at the bottom. For that particular final state, the cancellation is perfect if the two initial components have the same amplitude. However, not all final states can be reached by both particle and hole scattering. For example, if the particle ends up with a momentum that is not allowed in the final state, as illustrated below in fig. 13, there is no way to make that state by a collision of a hole. Note that the region of phase space which is effectively

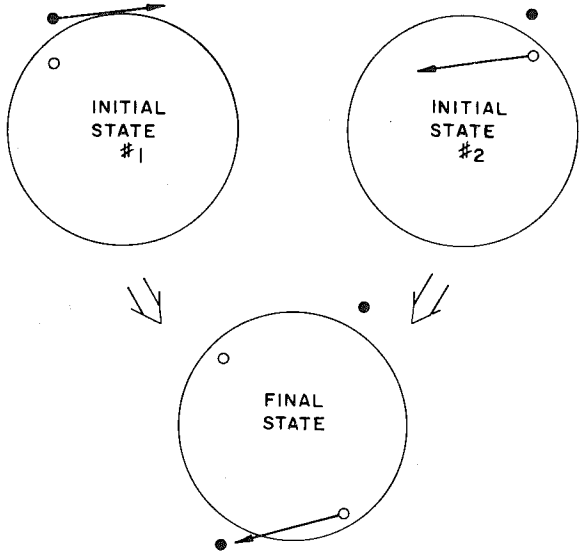

Fig. 12. Two particle–hole configurations which can lead to the same 2p–2h state.

excluded by the cancellation varies as $\cos\theta$. But this is just the shape of the excluded phase space in the double sphere geometry we considered earlier. Thus it is plausible to suppose that the coherence reduction factor in the double sphere geometry is the same as in the giant quadrupole state.

Since it was found that the collision rate decreased by a factor of 3 in the double sphere geometry, this model predicts that the width of the giant quadrupole should be smaller than the single-particle estimate by

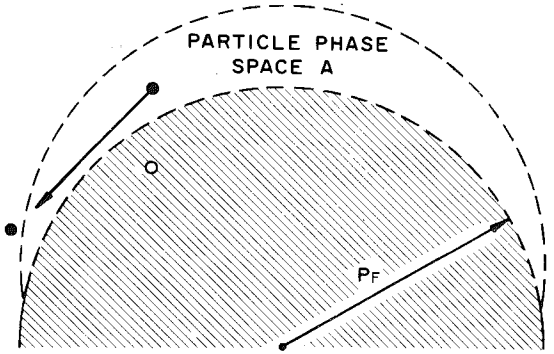

Fig. 13. Region of phase space which is effectively excluded.

this factor. In fact, the empirical reduction is only by a factor of 2, so the full coherence model is too crude. Some disagreement is to be expected: for one thing, the model assumes that the vibration is completely coherent, but in fact 12% of the sum rule in ^{208}Pb is contained in a low-lying state.

If a giant monopole state is ever found, it would provide an even better test of the mechanism of dissipation. In the collective description, the Fermi surface remains spherical, and merely expands and contracts. Thus there are no collisions allowed. In the shell model language, there should be complete cancellation between particle and hole.

6. Theory at low and medium energy

We are now ready to study the dynamics of low and medium energy collisions of nuclear matter. Let us begin with the behavior of infinite slabs, and later discuss the treatment of three dimensional geometry. The theory is relatively simple for the Vlasov equation, and the classical physics contained in this equation will be discussed first. However, there are several respects in which the classical theory is inadequate. As will be seen, when the system is described in a fully quantum mechanical way, it tends to break up into fragments much more easily than in the classical description. Also, quite energetic nucleons can emerge from the collision in the quantum theory.

6.1. Shock waves in one dimension

When two slabs collide, the evolution of the distribution function depends greatly on the nature of the self-consistent potential. In the Vlasov equation there are no collisions, but under suitable conditions a shock wave could form, mediated by the self-consistent potential. Under other assumptions about the potential, the two slabs would mix smoothly, with the interface between the mixed and unmixed parts spreading out indefinitely. These possibilities may be discussed starting from the following initial distributions:

$$f_1 = \theta(z - vt)\theta(|p - mv| - p_F)\,; \qquad f_2 = \theta(z + vt)\theta(|p + mv| - p_F)\,. \tag{6.1}$$

Before the nuclei collide, the self-consistent potential in the Vlasov equation keeps the distribution functions localized in coordinate space according to eq. (6.1). When the nuclei collide, the potential will change at the interface between the two nuclei. The simplest assumption we could make

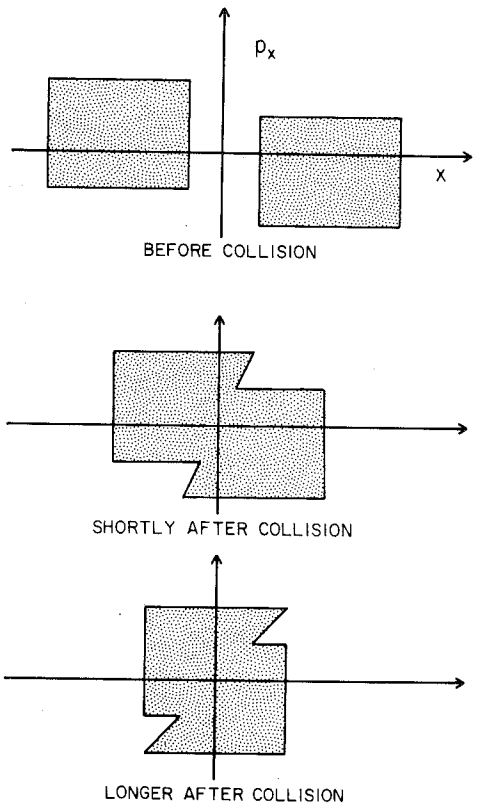

Fig. 14. Time evolution of the distribution function.

is that the potential in the overlap region becomes equal to the potential within the individual nuclei. Then the potential wall disappears and the distribution function evolves as shown in fig. 14, i.e., all of the particles in the interface region propagate as free particles. Notice that this has the appearance of a breaking wave: the fastest particles from one nucleus penetrate the other nucleus to a greater distance.

If the potential changes in the overlap region, the behavior will be more complicated, with the possibility of a shock wave forming. The discussion of the dynamics is simplified by noting that the density in phase space remains constant in the reference frame moving with the particles. This follows because the distribution function of the Vlasov equation satisfies Liouville's theorem. Since the initial condition, eq. (6.1) starts out with a density of either zero or one, this remains as time goes on. We then only

have to discuss the shape of the boundary separating these two regions of phase space. This can be done by following the dynamics of a particle located in the boundary, i.e. the Fermi surface in the initial state. Let us choose such a particle and label its coordinates in momentum space (p_x, p_y, p_z). Then the fact that it is on the Fermi surface implies

$$(p_z - mv)^2 + p_y^2 + p_x^2 = p_F^2 . \tag{6.2}$$

When this nucleon passes into the high density region, its momentum will only change in the z direction. In order to determine the charge in p_z, assume that in the high density region the self-consistent potential differs from the initial potential by an amount ΔU. Also, assume that the transition region between the initial distribution and the high density distribution moves with a velocity v_t. Then the principle of energy conservation in a reference frame moving with the transition region requires that the final momentum p_z' be related to the initial momentum p_z by

$$(p_z' + mv_t)^2 = (p_z + mv_t)^2 + 2m\Delta U . \tag{6.3}$$

Thus in the high density region the spherical distribution function is distorted into a spheroidal shape. There will be another spheroid in the overlap region arising from the other nucleus. These two shapes intersect if the incident energy is not too high. Of course the density remains unity in the region of intersection of the spheroids. This geometry is illustrated in fig. 11.

Whether or not a shock is formed, that is, whether the transition region remains sharp, can be determined from the sign of ΔU. Let us first consider positive (repulsive) ΔU. Then the velocity of the transition region must be greater than v_F if there is to be a higher density on the downstream side than on the upstream side.

Exercise. Show that $v_t > v_F$ if $\Delta U > 0$ and $\Delta p > 0$.

Let us now examine the distribution function moving in this frame with $v_t > v_F$. On the upstream side, the region of the incident nuclear matter, the distribution function does not touch the $p = 0$ axis, as shown in fig. 15. On the downstream side, the Fermi surface is given in eq. (6.3), and is sketched in fig. 15 as an egg shape.

We can consider the limit of a weak shock of this type, letting ΔU become small. Then eq. (6.3) may be solved for p_z' as

$$\begin{aligned} p_z' &= [(p_z + mv_t)^2 + 2m\Delta U]^{1/2} - mv_t \\ &\approx p_z + m\Delta U/(p_z + mv_t) . \end{aligned} \tag{6.4}$$

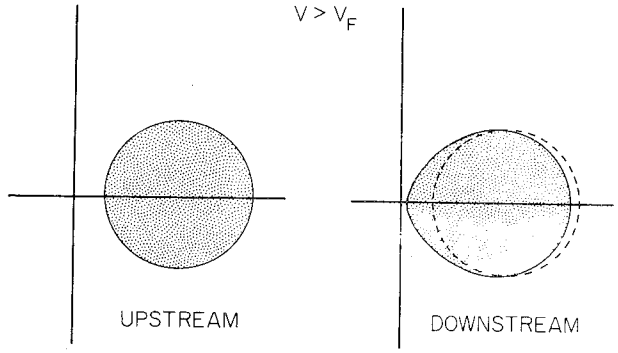

Fig. 15. Distribution function when $v_t > v_F$.

The boundary of the Fermi surface changes by an amount

$$p_z' - p_z = m\Delta U/(p_z + mv_t) . \tag{6.5}$$

In terms of the distribution function in spherical coordinates,

$$\Delta f(\boldsymbol{p}) \simeq \delta(p - p_F)\Delta p_z \cos\theta_{\hat{p}} = \delta(p - p_F)\frac{m\Delta U \cos\theta_{\hat{p}}}{\cos\theta_{\hat{p}} + v_t/v_F} . \tag{6.6}$$

This is exactly the form of distribution function obtained by Landau in describing small amplitude waves. Equation (6.6) shows that zero sound vibrations are the small amplitude limit of the shocks we are describing here.

The situation when ΔU is attractive is quite different. In this case, we can see easily that v_t must be less than v_F, or else the downstream side would have a lower density. The appearance of the distribution function in the frame moving with the transition region is shown in fig. 16. On the upstream side, the Fermi sphere now cuts the $p = 0$ axis. The particles to the right propagate into the overlap region, and gain energy by ΔU in crossing the transition. This is indicated by the right-most surface on the downstream graph. By a similar argument, the particles to the left propagate from the downstream to the upstream region and lose energy by just the right amount to complete the Fermi sphere. We have no information on the region on the downstream side indicated by question marks. It is highly implausible that conditions for such a shock could be set up. In Landau theory, corresponding to the small amplitude (ΔU small) limit, there are no stable waves when ΔU is attractive. It is most likely then that when ΔU is attractive or not too repulsive, the breaking wave picture of

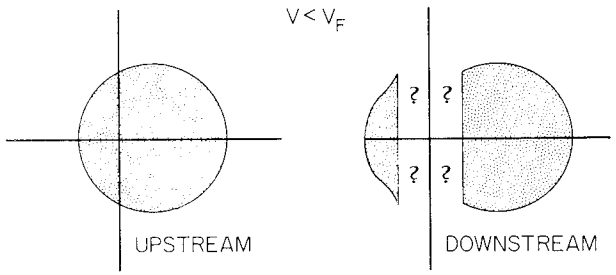

Fig. 16. Distribution function when $v_t < v_F$.

fig. 14 is valid. Assuming that the equation of state is known in the form of the relation between ΔU and $\Delta\rho$, the dynamics contained in eq. (6.3) can be used to relate the incident velocity of a collision to the maximum density. For example, in the trivial case where $\Delta U = 0$, a density of $\rho = 2\rho_0$ would be achieved at an incident projectile energy of $E/A = 4E_F \approx 152$ MeV. The time-dependent Hartree–Fock calculations of ref. [6.2] give a maximum density of $1.8\rho_0$ when the projectile energy is 200 MeV/A.

Problem. Determine the maximum density for projectiles of energy 200 MeV/A with the equations of state (4.1) and (4.6).

It is also of interest to consider the behavior of the rarefaction wave that follows the nuclear matter compression. The considerations are identical to those of the compressional shock wave. If the equation of state has

$$\Delta U/\Delta\rho > 0\,,$$

then the expansion process will be the reverse of the compression, and normal nuclear matter will emerge at the incident velocity. On the other hand, for the more dissipative compression that occurs when $\Delta U/\Delta\rho < 0$, the expansion is also dissipative and it is not clear what the Fermi surface would look like.

Study problem. Estimate the amount of energy dissipation occurring from the combined compression and expansion phases when $\Delta U = 0$.

Aside. In another field of many-body physics, plasma physics, collisionless shocks can also occur and have been studied theoretically [6.1]. For many purposes, the plasma may be considered as a gas of ions interacting by means of a potential. The electrons need not be considered explicitly:

they serve only to screen the interaction, making it short range. There is a great richness of behavior possible in plasmas. One feature is the existence of large amplitude stable solitary waves (solitons). In one type of shock wave, the potential U which is constant on the upstream side, develops a sinusoidal oscillation on the downstream side. There is also a repulsive step at the shock boundary.

6.2. Friction

There are a number of interesting topics that can be discussed with the behavior of the distribution function given. One subject that has received attention recently is the model for friction in which dissipation is obtained by particle transfer. We can discuss macroscopic concepts such as the position and momentum of the individual nuclei after the collision by arbitrarily assigning the particles on each side of the center of mass collision point to one or the other nucleus. The rate of transfer of momentum from one side to the other is given by

$$\mathrm{d}p/\mathrm{d}A\,\mathrm{d}t = \tau_{zz} = \int \mathrm{d}\boldsymbol{p} p_z v_z f(\boldsymbol{p})\,. \tag{6.7}$$

In the geometry of two intersecting spheres, fig. 11, the momentum transfer rate is

$$\mathrm{d}P/\mathrm{d}A\,\mathrm{d}t = [2\pi k_F^5/(2\pi)^3 m][x(1+x) + \tfrac{1}{3}(1+x^3)(1-x^2) - \tfrac{1}{2}x(1-x^4) - \tfrac{1}{5}(1+x^5)]\,, \tag{6.8}$$

where the separation between centers of the spheres is $P = 2p_F x$. In the limit of small x, this becomes

$$\mathrm{d}P/\mathrm{d}A\,\mathrm{d}t = [k_F^5/(2\pi)^2 m](\tfrac{2}{15} + \tfrac{1}{2}x + \cdots) = (k_F^2/2m)\rho(\tfrac{2}{5} + \tfrac{3}{2}x + \cdots)\,. \tag{6.9}$$

To this must be added the potential contribution to the momentum flux. By eq. (2.27) the contribution is

$$\mathrm{d}P/\mathrm{d}A\,\mathrm{d}t = U\rho - V\,. \tag{6.10}$$

At normal nuclear density this just cancels the constant term in eq. (6.9). This follows from the condition that the energy per particle be a minimum at normal density,

$$\frac{\mathrm{d}}{\mathrm{d}\rho}\left(\frac{E}{A}\right) = \frac{\mathrm{d}}{\mathrm{d}\rho}\left(\frac{3}{5}\frac{p_F^2}{2m} + \frac{V}{\rho}\right) = \frac{1}{\rho}\left(\frac{2}{5}\frac{p_F^2}{2m} + U - \frac{V}{\rho}\right) = 0\,.$$

Thus if the potential contribution, eq. (6.10), does not change with density, the momentum transfer rate is linear in the relative velocities of the nuclei. This is just the way a classical frictional force behaves. Swiatecki has advocated a formula derived from a classical model, of nucleons bouncing off a wall separating the two nuclei. Since there is no way to distinguish bouncing from free passage of nucleons in both directions, the equation he finds is equivalent to the linear term in eq. (6.9). Expressed in terms of the density of nucleons ρ, their mean velocity $\bar{v}$, and the relative velocity v_{rel}, the formula is

$$\mathrm{d}P/\mathrm{d}A\,\mathrm{d}t = m\rho\bar{v}v_{\mathrm{rel}}\,. \tag{6.11}$$

Exercise. Show that the contribution of the linear term in eq. (6.9) can be expressed in the form eq. (6.11).

6.3. *Fragmentation and escape of particles*

With the distribution function evolving according to the Vlasov equation, the two slabs will be brought to rest in the center of mass frame in a time about equal to the time it takes a particle at the Fermi surface to traverse the slab. After the particles reach the farther surface, a variety of things can happen. First, the extra pressure of the particles hitting the nuclear surface causes the nuclei to expand. If the collision energy is not too high, the nuclei will remain fused and the surfaces will oscillate about the equilibrium. At higher energies, the disturbance is sufficiently violent that a group of particles break off together. This is found to take place at incident slab energies greater than ~ 8 MeV/A, in both the time-dependent Hartree–Fock calculations [6.2] and in hydrodynamic calculations [6.3]. In fig. 17 is illustrated the TDHF calculation, at a projectile energy of 18 MeV/A. The first group of particles moves off with a higher velocity than the incident projectile. This effect is probably not contained in the classical treatment. When the particles from the projectile traverse the target, a standing wave is set up when they are reflected from the surface of the target. The nucleus will fracture at the weakest point, which is the node of a standing wave located a distance $\sim\pi/k_{\mathrm{F}}$ from the surface. Since there are no internal nodes in the z direction between the wall and this first node, the nuclear matter going off will have a nodeless internal structure in this direction, like an alpha particle or a light p-shell nucleus.

In the classical description, the way the break-up would come about is as follows. First, a collisionless rarefaction wave would propagate from the

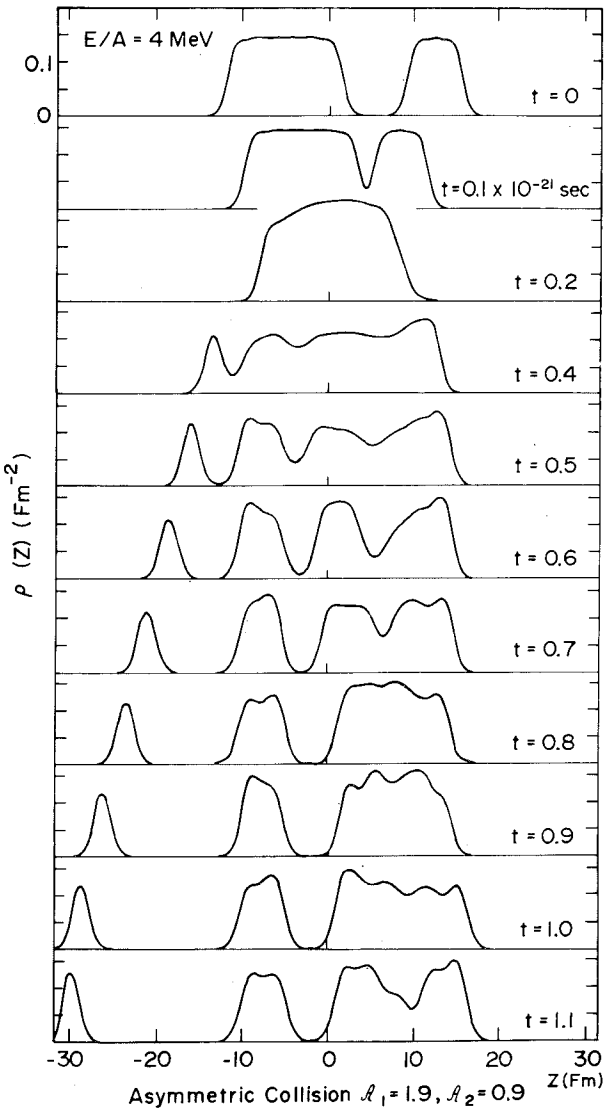

Fig. 17. Time-evolution of two colliding slabs in time dependent Hartree–Fock approximation.

surface back into the interior. When this met the rarefaction wave from the other side, the density would fall below nuclear matter density, as a double rarefaction wave propagated back toward the surface. If the density in this region were below the critical density, the matter would split up before this second wave proceeded very far.

Problem. Assuming that the first rarefaction wave restores the nuclear matter to normal density, estimate the threshold energy for this mechanism of breakup.

There is an additional effect associated with the particles of the projectile traversing the target nucleus. A fraction of these particles will have enough energy to escape from the farther edge of the target nucleus immediately. A first estimate of this effect may be made by adding the projectile velocity v_p to the Fermi velocity of the nucleons v_F. A nucleon at the Fermi level would have a kinetic energy in the lab given by

$$T_{lab} = \tfrac{1}{2}m(v_p + v_F)^2 . \tag{6.12}$$

If this kinetic energy exceeds the depth of the potential well, the nucleon can escape from the target nucleus.

Exercise. Show that the threshold for particle ejection is at a bombarding energy of 0.8 MeV/A.

This mechanism is quite distinct from the break-up of the nuclear matter, as it does not involve the dynamics of the potential field at all.

When quantum calculations of the emitted nucleons are made, it is found that the fraction of particles that escape this way is small, on the order of a few tenths of a percent at a projectile energy of 10 MeV/A, but that the energy of these particles can greatly exceed the classical estimate, eq. (6.11). It turns out that the speed at which the nuclei approach is important also for determining the distribution in energy of the particles travelling through the other nucleus. If the nuclei approach slowly, the potential changes adiabatically and the particles have the same energy propagating through the second nucleus as they had in the first. If the nuclei collide at high velocity, the potential changes rapidly and the particle wave-functions are not as close to being energy eigenstates. It would be interesting to observe these fast particles experimentally to confirm this feature of the dynamics. Unfortunately, energetic particles can also be produced in peripheral collisions from the decay of excited states of the

projectile. An experimental test would therefore require that central collisions were positively identified.

6.4. *Threshold pion production*

Another application of the one-dimensional dynamics is to threshold pion production. In this case, the dynamic assumptions are minimal. We represent the distribution function in the overlap region by two intersecting spheres. Pions are produced by collisions between nucleons in this geometry. The endcaps on the distribution function provide the energetic nucleons needed to create pions. The distribution function eventually thermalizes, and the statistical equilibrium is such that fewer pions are produced without the endcaps. Of course, all of this neglects coherent mechanisms for pion production, such as considered in refs. [6.4] and [6.5].

We shall neglect the pion production after the distribution function has thermalized. We shall also neglect the greater complexity of the distribution function in the transition region. The occupation probability of the endcaps on the distribution function will then be given by

$$\exp[-(\tfrac{1}{2}vt \pm z)\langle\sigma^N\rho_0\rangle]\begin{cases} p_z < 0 \\ p_z > 0 \end{cases} \tag{6.13}$$

where v is a relative velocity. The inverse decay length, $\langle\sigma^N\rho_0\rangle$ is the same as in sect. 5. The pion production rate from pairs of nucleons in the two endcaps is then given by

$$\mathrm{d}n_\pi/\mathrm{d}t = v\sigma^\pi \exp[-(\tfrac{1}{2}vt + z)\sigma^N\rho_0] \exp[-(\tfrac{1}{2}vt - z)\sigma^N\rho_0] \times \rho(\tfrac{1}{2}vt + z)\rho(\tfrac{1}{2}vt - z) . \tag{6.14}$$

where σ^π is a pion production cross-section normalized to the phase space geometry we have considered. It is trivial to integrate over z, to obtain a production cross-section per unit area of the colliding slabs.

$$\mathrm{d}N/\mathrm{d}t\,\mathrm{d}A = v^2t\rho_0^2 \exp(-vt\langle\sigma^N\rho_0\rangle)\sigma^\pi . \tag{6.15}$$

We next integrate over time to get the total number of pions produced for slabs with area A:

$$N = \frac{\sigma^\pi}{(\sigma^N)^2} A . \tag{6.16}$$

This simple formula can be understood as follows: the number of pions

produced is the product of the probability of an individual nucleon producing a pion, σ^π/σ^N, multiplied by the number of nucleons which can make an initial collision, A/σ^N. This calculation will not be reliable in the surface region, because the phase space is not completely filled in the surface. It is therefore important to see whether the decay of the endcaps is sufficiently slow that pion production takes place when the nuclei overlap. The mean overlap wh a pion is produced can be calculated as

$$\int \frac{vt(\mathrm{d}N/\mathrm{d}t)\,\mathrm{d}t}{N} = \frac{2}{\sigma^N \rho_0}\,. \tag{6.17}$$

Since $1/\langle\sigma^N\rho_0\rangle$ is ~ 2 fm or larger, the mean penetration is substantial. Thus, pion production should sample the nuclear interior.

Equation (6.16) may be used to get a production rate if the mean overlap area per collision is known. This can be estimated from simple geometry: considering collisions of ^{20}Ne on ^{238}U the mean area is about $A \approx 10$ fm^2. Also, the relationship between the incident energy and the geometry of the momentum space distribution function is needed. The simplest assumption is that the potential field does not change as the density increases. Then for a typical collision of 200 MeV/A, the separation of the centers of the Fermi spheres is $P = 2.28\, p_F$, i.e. the spheres do not touch. In this geometry the cross-sections work out to $\sigma^\pi \approx 10^{-2} \times \sigma^N$ and $\sigma^N \approx 2$ fm^2. Inserting all this in eq. (6.16), the probability of producing a pion in a collision is $\approx 1/20$. The estimate is clearly dependent on the assumed equation of state. If the nuclear matter had a stiff equation of state, the potential well would become repulsive and the distribution function would have a much more compact shape. This would imply a small pion production cross-section.

6.5. *Three dimensions*

The increased degrees of freedom in three dimensions offers the promise of a greater dependence of the reactions on the assumed equation of state. However, theory in three dimensions is very difficult. The time-dependent Schrödinger equation can be solved in two dimensions only with great effort. A three-dimensional calculation has been made for the system [6.6] ^{16}O + ^{16}O, but the treatment of medium- or heavy-weight systems seems beyond the capabilities of present-day computers. However, much of the physics can be simulated with approximations that make use of special coordinate systems. For example, 3-D calculations are done assuming

axially symmetric wavefunctions in a coordinate system along the line of centers of the two nuclei. An even simpler approximation is that the wavefunction is separable in this coordinate system. This is true for the particles in light nuclei, which are well represented by harmonic oscillator functions. Only the wavefunction in the z-direction, along the line of centers, is allowed to change with time. Since none of these methods have been applied to the really heavy systems which show the strong damping phenomenon so clearly, it is well to consider other methods first.

Nix and collaborators have pursued the pure hydrodynamic description. One needs to trace the shape, density, and velocity fields as a function of time. Nix developed a 5-parameter description of the shape of the surface of two fused nuclei [6.7]. At low energies, the flow is nearly incompressible, so we need not consider the density explicitly. If the flow is also irrotational, then there is a scalar velocity potential and the velocity field at all points is determined from knowledge of the surface motion. Then in principle the entire dynamics can be expressed in terms of equations of motion for the surface degrees of freedom.

To formulate the continuum mechanics, we write down the pressure tensor, eqs. (2.27–8),

$$P_{ij} = \delta_{ij}(U\rho - V) + (1/m)\langle(p_i - \bar{p}_i)(p_j - \bar{p}_j)\rangle\,. \tag{6.18}$$

The first term is the central potential, and the second term is the anisotropic pressure coming from a distorted Fermi sphere. This term depends on the previous history of the system. From eq. (2.52) the rate at which an anisotropic Fermi surface develops from a spherical Fermi surface is proportional to the rate of shear of the flow. However, there is also a relaxation of the Fermi surface back to spherical shape, due to the damping mechanisms. Thus we may express the anisotropic part of the pressure tensor as

$$\frac{D}{Dt}\langle p_i v_j\rangle = -\frac{1}{2}\frac{\langle p^2\rangle}{3m}(\nabla_i v_j + \nabla_j v_i) + \left(\frac{D}{Dt}\langle v_i v_j\rangle\right)_{\text{relaxation}} \tag{6.19}$$

The dissipation is complicated because as we saw in previous sections, there are two dissipation mechanisms that operate on different time scales. The ballistic propagation of the particles smooths out $\langle p_i p_j\rangle$ on a time of the order of the transit time for a nucleon at the Fermi surface. The rate at which the uniform Fermi surface is approached can be assumed to be proportional to the deviation from uniformity. Thus:

$$\left(\frac{D}{Dt}\langle p_i v_j\rangle\right)_{\text{one-body}} = \frac{-1}{\tau_1}\left(\langle p_i v_j\rangle - \langle\overline{p_i v_j}\rangle\right), \qquad \text{with } \tau_1 \approx L/v_F\,. \tag{6.20}$$

The two-body collisions restore the distribution function to a spherical shape on a different time scale. The infinite matter estimates of sect. 5 indicate that the relaxation rate is proportional to the square of the deviation from spherical,

$$\left(\frac{D}{Dt}\langle p_i v_j\rangle\right)_{\text{two-body}} = -\frac{1}{\tau_2}\left(\langle\overline{p_i v_j}\rangle - \tfrac{1}{3}\delta_{ij}\sum_i \langle p_i v_i\rangle\right)^2 . \tag{6.21}$$

If a linear relaxation rate is used in eq. (6.21), it is possible to derive ordinary linear viscosity. It is necessary to assume that accelerations are small and that the two time constants are equal,

$$\tau_1 = \tau_2 = \tau \ll v_i/\dot{v}_i .$$

Then eq. (6.20) can be integrated to

$$\langle p_i v_j\rangle = -\tfrac{1}{2}\tau(\nabla_j v_i + \nabla_j v_i)\cdot\langle p^2\rangle/3m . \tag{6.22}$$

This is just the stress tensor for ordinary viscosity: the coefficient of viscosity η is related to the shear modulus μ and the relaxation time τ by

$$\eta = \frac{\langle p^2\rangle}{3m}\tau \approx \frac{p_F^2}{5m}\rho\tau = \mu\tau . \tag{6.23}$$

In the literature there are reported calculations of nuclear hydrodynamics using the coefficient of ordinary viscosity as an adjustable parameter [6.8]. The energy dissipation observed in fission determines the value of this parameter to be $\approx 0.02\,\hbar\,\mathrm{fm}^{-3}$. The hydrodynamic model with $\eta \approx 0.02\,\hbar\,\mathrm{fm}^{-3}$ also gives a reasonable account of the energy dissipation in the collisions of heavy nuclei. However, the hydrodynamic description predicts rather complete fusion of the nuclei during the course of the collision. When the nuclei separate, the two fragments are more nearly equal in mass than is observed. It seems plausible that an improved description of the dissipation, incorporating the longer memory time for the quadrupole distortions, would predict less equilibration in mass.

Exercise. Make a numerical extimate of η, taking the time constant in eq. (6.22) from the width of the giant quadrupole state of ^{208}Pb.

Study problem. The hydrodynamic model of ref. [6.7] assumes irrotational flow. How can a rotational velocity field be added to this formalism? Are the equations of motion for the irrotational part of the flow modified by this addition?

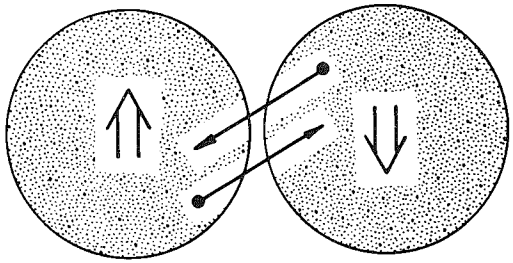

Fig. 18. Transfer of angular momentum in a grazing collision.

6.6. *Angular momentum transfer*

Angular momentum transfer can only be discussed in the framework of a model that contains rotational flow. Qualitatively, it is clear what will happen to the distribution function in a grazing collision. There will be a transfer of nucleons which carries tangential momentum, as illustrated in fig. 18. These nucleons bounce off the sides of the nuclei they pass into, producing odd shapes in the fully three-dimensional quantum calculations [6.6]. The rate of tangential momentum transfer can be estimated by examining the distribution function in the overlap region during an off-center collision. If there is only tangential motion, the distribution function at the point of contact of the two nuclei will have the shape given in fig. 19, where $2x$ is the relative momentum per particle of the two nuclei. Defining the z axis to be along the line of centers, and the x axis to be along the relative momentum vector, the rate of tangential momentum transfer is given by the integral $\tau_{xz} = \int \mathrm{d}\boldsymbol{p} p_x v_z f(\boldsymbol{p})$. Swiatecki finds this rate to be half the rate of longitudinal momentum transfer, for the same relative velocity. However, the ratio of radial to tangential momentum transfer offers the possibility of measuring the equation of state. Only the radial momentum transfer depends on the potential field. Thus, if the relative amount of radial momentum transfer were large, it would indicate a stiff equation of state.

Problem. Verify that the tangential momentum transfer for the geometry in fig. 19 is half the longitudinal momentum transfer for the geometry of fig. 11.

Study problem. Determine the dependence of the radial to tangential friction on the coefficient σ in the equation of state.

To get a total transfer rate, we need to know the area of contact of the two nuclei. Since particles at the nuclear surface can easily tunnel from

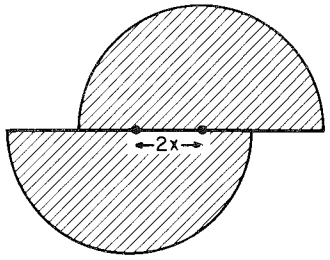

Fig. 19. Distribution function in the case of a tangential motion.

one nucleus to the other, it is clear that quantitative calculations of angular momentum transfer will require a careful treatment of the quantum mechanics.

Probably the most direct information on the equation of state will come from a study of the distribution in momenta of the products of the collision. One could think of defining a distribution function for a final state $f(p)$, and characterizing it by a multipole decomposition. If the collision products were numerous enough, each collision could define the low moments of such an f. If one studies the low momentum portions of f, for most collisions the density should be oblate, with the beam axis in the high density region. This is because the collisions will be at moderately large impact parameter, and the products will come out in the plane of the reaction. A small proportion of collisions will be at small impact parameter and will not have this pancake distribution of low energy products. For these events a study of the high energy particles should be illuminating. One possibility is that there be enhanced production of high momentum in the transverse direction from the beam. Such a phenomenon occurs in hydrodynamics when two surfaces collide. This is the phenomenon responsible for the jet in shaped explosive charges. In several theoretical works on heavy ion collisions, it was speculated that this effect might occur [6.9, 6.10]. However, the phenomenon requires that the pressure tensor become isotropic, which only happens in the time scale of two-body collisions. The lecturer feels that the mean free paths are too large for this collective acceleration to occur.

If energetic particles are seen along the beam axis preferentially in the small impact parameter collisions, this would be good evidence for the single particle dynamics discussed in the section on the one-dimensional slab, sect. 7.2.

7. High energy theory

7.1. Phenomenology of nucleon–nucleon and nucleon–nucleus collisions

The most naive picture of high energy collisions is that the nucleons in the target and projectile scatter independently. This model has been tested directly by comparing cross-section data for various projectiles and targets. One experiment compared pion production with proton, deuteron and alpha projectiles [7.1]. The energy of the projectiles was 2.1 GeV/A. The overall production rate at forward angles behaved as expected in this model, i.e. twice as many pions were produced from alphas as from deuterons. However, the energy distribution had a high energy tail for the more complex projectiles. In the case of the deuterons, the energy distribution could be understood quite well in terms of the spread in momentum of the nucleon in the deuteron. This model explained differences in cross-section of 3 orders of magnitude to better than a factor of 2.

Particles are seen in a region kinematically unfavored in nucleon collisions when complex nuclei are bombarded by high energy protons. In an experiment with 400 GeV protons in nuclear emulsion [7.2], the probability of relativistic pions emerging in the backward hemisphere was found to be proportional to the number of heavily-ionizing fragments produced in the collision. This probability was $\frac{1}{3}$ for central collisions on AgBr.

One warning about collisions at the highest energies: the number of secondary particles in collisions at extremely high energy appears to be less than cascade models would predict [7.3]. The present understanding is that it takes some time to materialize the secondary particles after the nucleon is excited. Until these secondaries have materialized, they do not scatter independently.

The most basic quantities to be calculated in heavy ion collisions are the energy and momentum transfers between projectile and target. To calculate these in the independent scattering model, knowledge of average cross-sections and momentum transfers for nucleon–nucleon collisions is needed. Above 200 MeV lab energy, the total nucleon–nucleon cross-section averaged over neutrons and protons decreases to a minimum of 25 mb, and then increases to a plateau of about 45 mb above the meson production threshold. In this plateau region, about half the cross-section is elastic scattering and half is inelastic with one or more pions produced. To compute the average momentum transfer, consider a collision with an initial projectile momentum p_{in}, and a center of mass scattering angle θ_{cm}. Then the longitudinal momentum transfer is given by

$$\delta p_{\parallel} = \tfrac{1}{2} p_{\mathrm{in}}(1 - \cos\theta_{\mathrm{cm}}) .$$

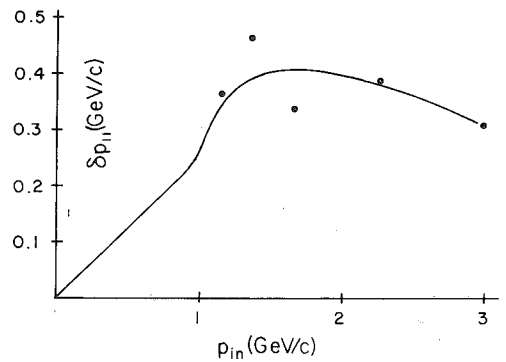

Fig. 20. Longitudinal momentum transfer.

This expression looks non-relativistic, but is true relativistically as well. The average momentum transfer is then given by

$$\langle \delta p_{\parallel} \rangle = \frac{1}{\sigma} \int_0^{90^\circ} \mathrm{d}\Omega \, \frac{\mathrm{d}\sigma}{\mathrm{d}\Omega} \, \tfrac{1}{2} p_{\mathrm{in}} (1 - \cos \theta_{\mathrm{cm}}) \,. \tag{7.1}$$

When the incident momentum is above 1 GeV/c, half the cross-section goes into pion production and we have to decide how to include the momentum of the pions. One point of view is to say that the pion is lost to the system and neglect it in the equation. Another point of view is to assume that the pion is always correlated with a nucleon in a Δ resonance. The reaction can be treated with two-body kinematics, with the final state $p\Delta$ or $\Delta\Delta$ when one or two pions are produced. This seems reasonable for collisions up to about 2 GeV bombarding energy. In fig. 20 we give the results of the computation of eq. (7.1) at several different energies, assuming two-body kinematics. The nucleon–nucleon cross-sections needed for this graph were obtained from a compilation [7.4]. At low energy, below 1 GeV/c incident momentum (300 MeV energy), the cross-section is roughly isotropic, and the longitudinal momentum transfer is proportional to the incident momentum,

$$\langle \delta p_{\parallel} \rangle \simeq \tfrac{1}{4} p_{\mathrm{in}} \,.$$

From the figure we see that the momentum transfer rises up to a maximum of about 0.4 GeV/c per collision, and then seems to fall at higher energies. There is considerable scatter in the points around 1.5 GeV/c. The elastic cross-section is changing in this region, and the Δ production is moving away from threshold and becoming forward peaked. The momentum

transfer in the transverse direction is best characterized by its mean square. The relativistic expression for this is

$$p_{\perp}^2 = t(1 + \cos \theta_{\mathrm{cm}}) \,,$$

where t is the Lorentz scalar

$$t = |\boldsymbol{p} - \boldsymbol{p}'|^2 - (E_p - E_{p'})^2 \,.$$

At the lower energies the momentum transfer from isotropic scattering is

$$\langle p_{\perp} \rangle^2 = \tfrac{1}{6} p_{\mathrm{in}}^2 \,.$$

Above 1.3 GeV/c incident momentum, the elastic scattering is strongly forward peaked. The peak is fit quite well by the expression,

$$\mathrm{d}\sigma/\mathrm{d}t = A \exp(-bt) \,, \tag{7.2}$$

with

$$b \approx 9(\mathrm{GeV}/c)^{-2} \,.$$

This same exponential fall-off is found in inelastic scattering as well. The mean square transverse momentum is then

$$\langle p_{\perp}^2 \rangle \simeq 2/b \approx 0.22\,(\mathrm{GeV}/c)^2 \,. \tag{7.3}$$

Problem. Determine the average longitudinal momentum transfer in proton–proton collisions at 12 GeV, using the data of Nucl. Phys. B69 (1974) 454.

7.2. *One-dimensional slab model*

The evolution of the nucleon distribution function for heavy ion collision will first be examined in a one-dimensional model, considering the collision of two slabs. Providing the momentum distribution of the nucleons in the projectile is well separated from the momentum distribution of the target, we can treat these as two distinct systems. Since the Fermi momentum is 300 MeV/c, the criterion is that the projectile momentum is much greater than twice this value. For a first calculation, we can study the behavior of the average momentum $\langle p \rangle$ as a function of position. The evolution of the average momentum during the course collision can be traced using the empirically determined momentum transfer from nucleon–nucleon collisions. Since each nucleon in the projectile will collide with many nucleons in the target, we first need an estimate of the mean number of collisions.

In terms of the nucleon–nucleon cross-section σ, the radius of the target nucleus R, and the density of nuclear matter ρ, the mean number of collisions is

$$\bar{n} = \sigma\rho 2\pi \int_0^R r\,\mathrm{d}r 2(R^2 - r^2)^{1/2}/\pi R^2 = \tfrac{4}{3}\sigma\rho R\,. \tag{7.4}$$

For the nucleus U, the radius is $R \simeq 7.2$ fm. With this value for the radius, the density of nuclear matter in the nucleus is $\rho \approx 0.152\ \mathrm{fm}^{-3}$. Assuming a cross-section of 40 mb, eq. (7.4) yields an average of 5.7 collisions. If we start with a projectile momentum of 3 GeV/c, each collision will lose an average of say 0.35 GeV/c, and the projectile nucleons will have 1 GeV/c momentum left. Starting with a lighter target, say $A \approx 100$, as would be found in nuclear emulsion, the number of collisions is 4.2 and the momentum remaining in the projectile nucleons will be 1.5 GeV/c. Thus the projectile particles will emerge in a broad forward cone.

Knoll and Hüfner [7.14] have extended this type of analysis to consider the spread in momentum as well as the behavior of the mean momentum. Their treatment is couched in a slightly different language from that of the distribution function. The longitudinal dimension of the nucleus is broken up into segments 1.8 fm long. This number is chosen because the mean volume per nucleon is $(1.8\ \mathrm{fm})^3$. The evolution of the phase space in each segment is represented by a nucleon in that segment, having a momentum spread of the Fermi momentum. The segments are numbered, and they consider the mean momentum of each segment of the target slab the projectile slab,

$$\langle p\rangle_{n_\mathrm{t}}\,, \qquad \langle p\rangle_{n_\mathrm{p}}$$

Here the segments in the target and projectile are labeled by n_t and n_p respectively. The other variables in the calculation are the longitudinal and transverse dispersion in momentum:

$$\sigma_\parallel(n) \equiv \langle (p_\parallel - \langle p_\parallel\rangle)^2\rangle_n\,; \qquad \sigma_\perp(n) \equiv \langle (p_\perp - \langle p_\perp\rangle)^2\rangle_n\,. \tag{7.5}$$

In the model, each segment of the projectile collides with each segment of the target. The changes in the above quantities after each collision are calculated as follows. For the change in mean momentum of segment n_p following collision with segment n_t, momentum conservation requires that

$$\Delta\langle p\rangle_{n_\mathrm{p}} = -\Delta\langle p\rangle_{n_\mathrm{t}}\,. \tag{7.6}$$

This change is assumed to be proportional to the difference in the momenta with the proportionality constant α

$$\Delta\langle p\rangle_{n_\mathrm{p}} = \alpha(\langle p\rangle_{n_\mathrm{t}} - \langle p\rangle_{n_\mathrm{p}})\,. \tag{7.7}$$

The dispersion in longitudinal momentum changes for three reasons. Probably most important, the scattering to different angles results in a dispersion. Also, for scattering to a given angle, the dispersion in transverse momentum is partially rotated to give a dispersion in longitudinal momentum. Finally, because the model assumes that the momentum changes by a constant fraction, the dispersion in $\sigma_\parallel$ will decrease as the momentum is transferred. These last two effects can be parameterized as

$$\Delta\sigma_\parallel = -2\alpha\sigma_\parallel + \alpha(\sigma_\perp^\mathrm{t} + \sigma_\perp^\mathrm{p})\,, \tag{7.8}$$

when the scattering angle is small and the dispersions are small compared to the momentum difference. The change in transverse dispersion is determined by a similar argument using a small angle scattering approximation. The result is

$$\Delta\sigma_\perp = -2\alpha\sigma_\parallel + \tfrac{1}{2}\alpha[\sigma_\perp^\mathrm{t} + \sigma_\perp^\mathrm{p} + \sigma_\parallel^\mathrm{t} + \sigma_\parallel^\mathrm{p} + (\langle p\rangle^\mathrm{t} - \langle p\rangle^\mathrm{p})^2]\,. \tag{7.9}$$

The initial conditions for the momenta in each segment are:

$$\langle p\rangle_{n_\mathrm{t}} = 0\,; \qquad \langle p\rangle_{n_\mathrm{p}} = p_\mathrm{in}\,;$$
$$\sigma_\parallel = \sigma_\perp = \tfrac{1}{5}p_\mathrm{F}^2\,. \tag{7.10}$$

The final energy-angle distribution of the protons is analyzed assuming that each segment is a Gaussian in momentum space, characterized by the final values of $\langle p\rangle$, $\sigma_\perp$ and $\sigma_\parallel$ that emerge from the calculation. The model can be compared with the data on ^{20}Ne collisions with U, at energies of 250 to 400 MeV/c. The spectrum of protons in the model is continuous, with the higher energy protons from the target overlapping the lower energy protons from the projectile. At forward angles, the spectrum of protons is nearly uniform in energy from 40–200 MeV. At backward angles, the energy spectrum falls off steeply. The agreement with the experimental inclusive spectrum is better than a factor of 2, for data that varies over more than two decades. Knoll and Hüfner point out that the final spectrum looks statistical, with a broad range of energies, but this happens not because of complete thermalization but because the different segments at different impact parameters have quite different mean energies.

The model predicts a gap in the proton energy spectrum for collisions at 2.1 GeV/A bombarding energy, with the protons from the projectile only

extending down to 1 GeV/c momentum. This agrees with the simple considerations we made earlier, but experimentally no gap has been seen in the proton spectrum.

A more serious possible deficiency of the model is the neglect of the interaction of the different segments within the target or within the projectile on each other. We would expect that particles would be ejected in the backward direction from a collision of a thin slab on a thick slab: the mean momentum of the trailing edge of the impinging slab would eventually become negative due to the pressure generated in the collision. This requires explicit consideration of the effect of one segment on another. In the present model, all of the projectile segments move through all of the target segments, which certainly could not happen if negative momentum were to be generated.

To estimate the number of particles coming off in the backward direction, we can apply ordinary hydrodynamics. The incident slab will create a shock, and a rarefaction wave will begin at the back end of the slab when the shock reaches it. This occurs when the incident slab has shocked an equal amount of material in the target. Thus, the velocity of this shocked material, v', would be half the initial velocity, $v_{\rm in}$. The internal energy per particle in the shocked material is related to the initial velocity by

$$I = \tfrac{1}{2}(E_{\rm in} - \tfrac{1}{2}mv'^2) = \tfrac{1}{4}mv_{\rm in}^2 . \tag{7.11}$$

Particles in the rarefaction wave have a maximum velocity of $3c$, where c is the sound velocity in the shocked material. Ignoring terms in the equation of state besides the internal energy, the sound velocity in the shock is

$$\begin{aligned} c^2 &= \gamma(\gamma - 1)I/m \\ &= \tfrac{5}{18}\, v_{\rm in}^2 . \end{aligned}$$

Thus the maximum velocity in the backward direction is

$$v_{\rm max} = 3c - v' = 0.58 v_{\rm in} . \tag{7.12}$$

The rarefaction would continue until the leading edge reached the front of the shocked region. The total amount of matter travelling backwards may then be estimated as the fraction of the rarefaction wave having particle velocity greater than $v_{\rm in}/2$, when the total amount of matter contained in the wave is somewhat greater than twice the incident matter.

Problem. Estimate the amount of matter travelling backwards, using the self-similar hydrodynamic rarefaction wave [7.5].

7.3. *Hydrodynamic models in three dimensions*

Although the mean free paths are too long for hydrodynamic equilibrium to be a good approximation, it is useful to study the hydrodynamic limit more closely, because differences in predictions that could be verified experimentally would be informative. Relativistic hydrodynamics does not introduce any difficulties in the formulation of the dynamics. The three conservation laws remain unchanged in any given coordinate frame. However, the equation of state will relate the pressure to the energy density in one particular coordinate system, the one moving with the medium. Thus a Lorentz transformation is necessary to relate the rest frame quantities to those in the lab frame. Labelling the rest frame energy and pressure by ε and p, the lab frame momentum M and energy densities E are:

$$M = \gamma^2(\varepsilon + P)\beta ; \qquad E = \gamma^2(\varepsilon + P) - P . \tag{7.13}$$

This may be shown by applying a Lorentz transformation to the energy–momentum tensor density. Numerical studies have been made in three-dimensional geometry by Amsden et al. In an initial calculation [7.6], the non-relativistic equation of state eq. (4.2) was used, with the pressure P related to energy ε and number density n by

$$P = [-\tfrac{2}{3}m_0(n/n_0) - \tfrac{1}{3}a(n/n_0)^2 + b(n/n_0)^{8/3}] + \tfrac{2}{3}\varepsilon . \tag{7.14}$$

The numerical method used to solve these equations has the space divided up into cells. Marker particles are placed in these cells to represent the fluid: the density in a cell is proportional to the number of marker particles in that cell. The calculation proceeds in a two-step cycle: in the first step, the particles are propagated to new positions, according to a position and velocity vector associated with each particle. In the second step, the new density is used to compute a pressure. The velocity vectors of the particles are changed according to the acceleration from the pressure gradient. Figure 21 illustrates the course of a head-on collision of 2.1 GeV/A ^{16}O nuclei on ^{107}Ag. The calculation is done in the rest frame of the ^{107}Ag, and the ^{16}O appears Lorentz-contracted. There is obviously a shock propagated outward from the point of contact. When the shock reaches the surface, a rarefaction ensues. Note that particles go off at high velocities in non-forward directions. Also, there are some particles going off sideways and backwards.

Study Problem. What is the maximum backward velocity in the case of a relativistic shock?

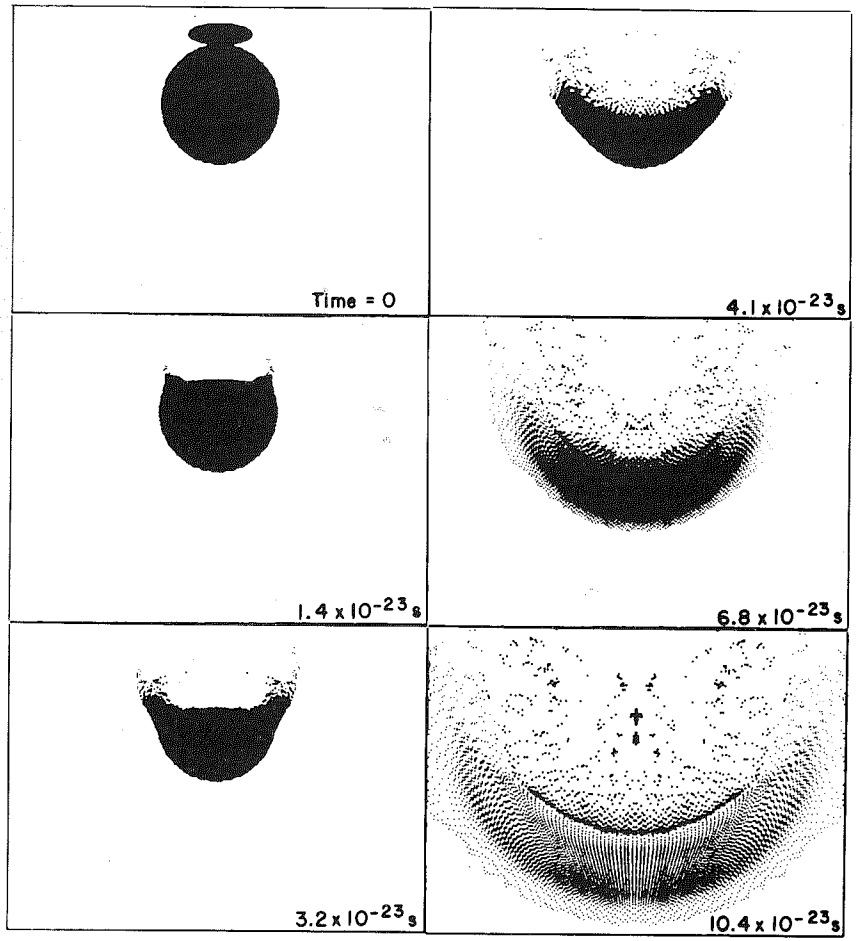

Fig. 21. Head-on collision of 2.1 GeV/A ^{16}O nuclei on ^{107}Ag.

As mentioned earlier, the hydrodynamic hypothesis of a short mean free path is quite unrealistic: the momentum distributions of target and projectile are not expected to equilibrate even for rather large nuclei. A generalization of the model to meet this deficiency is the hydrodynamics of two weakly interacting fluids. A formulation of this model has been given by Amsden et al. [7.7]. As before, the hydrodynamics is expressed in the three conservation laws and the equation of state. The number conservation law applies for the two fluids independently. The momentum and

energy conservation laws are modified to allow interchange between the two components. This may be expressed as follows for fluid i ($i = 1$ or 2):

$$(\partial/\partial t)\boldsymbol{M}_i + \nabla\cdot(\boldsymbol{\beta}_i\boldsymbol{M}_i) = -\nabla P_i - \partial\boldsymbol{M}_i^{(j)}/\partial t\ ; \tag{7.15}$$

$$(\partial/\partial t)E_i + \nabla\cdot(\boldsymbol{\beta}_i E_i) = -\nabla\cdot(\boldsymbol{\beta}_i P_i) - \partial E_i^{(j)}/\partial t\ . \tag{7.16}$$

Here $\boldsymbol{M}_i$, E_i, $\boldsymbol{\beta}$ and P_i are the momentum density, energy density, flow velocity and pressure of the fluid i in the laboratory coordinate frame. The rate of momentum and energy transfer from fluid j to fluid i is given by $\boldsymbol{M}_i^{(j)}$ and $E_i^{(j)}$. To derive expressions for $\partial M_i^{(j)}/\partial t$, and $\partial E_i^{(j)}/\partial t$, we start with the expression for these quantities in the rest frame of fluid j. The rate of momentum transfer is

$$\left.\frac{\partial M_i^{(j)}}{\partial t}\right|_{\beta j=0} = N_i n_j \beta\sigma\langle\Delta p_\parallel\rangle\ , \tag{7.17}$$

where N_i is the number density of fluid i, n_j is the density of fluid j, β is the relative velocity, σ is the cross-section and $\langle\Delta p_\parallel\rangle$ is the average longitudinal momentum transfer per collision. The energy transfer rate is given by a similar expression. The momentum and energy are not independent: in the nucleon–nucleon center of mass frame, there will be no energy transfer. The nucleon in the center of mass frame has a velocity

$$\beta_{\rm cm} = \beta\gamma/(1+\gamma)\ . \tag{7.18}$$

If a Lorentz transformation of $\beta_{\rm cm}$ is applied to the momentum transfer in the center of mass frame, the resulting 4-vector will be the momentum and energy transfer in the rest frame of one of the nucleons. The result is that the energy transfer is related to the momentum transfer by

$$\delta E|_{\beta=0} = \beta_{\rm cm}\delta P|_{\beta=0} = [\beta\gamma/(1+\gamma)]\langle\delta p_\parallel\rangle\ . \tag{7.19}$$

The 4-vector $(\partial E_i^{(j)}/\partial t,\ \partial\boldsymbol{M}_i^{(j)}/\partial t)|_{\beta=0}$ can then be transformed to an arbitrary frame for use in eqs. (7.15) and (7.16). The result for the momentum transfer is

$$\partial M_i^{(j)}/\partial t = \gamma_2\gamma\beta n_i n_j\sigma\langle\delta p_\parallel\rangle[1 - \beta\beta_j\gamma/(1+\gamma)]\ . \tag{7.20}$$

This expression is equivalent to

$$\partial M_i^{(j)}/\partial t = (\gamma_i\beta_i - \gamma_j\beta_j)n_i n_j\sigma\langle\delta p_\parallel\rangle\ . \tag{7.21}$$

The corresponding expression for the energy transfer is

$$\partial E_i^{(j)}/\partial t = (\gamma_i - \gamma_j)n_i n_j\sigma\langle\delta p_\parallel\rangle\ . \tag{7.22}$$

Expressed in this form, momentum and energy conservation are explicit. At the time of writing, numerical calculations with these equations have not been reported. We expect little difference in the predictions in the forward direction, since various models ranging from the cascade to the simple hydrodynamic model give similar results [7.8]. In the backward direction, there are differences between the models which ought to be resolved with the more refined approximation.

7.4. Composite particle abundances

As discussed in the first section, many composite particles are observed in the high energy collisions. For example, at forward directions in one high energy reaction there is approximately one deuteron for every two protons. A first model for the production of these light composite particles is to assume that thermodynamic equilibrium is established among the various species [7.9]. This of course requires that the interaction of the different species be neglected, which demands that the equilibration take place at rather low density. To derive the formula for the abundances of the various nuclei, we write the density of nuclei of a given type as an integral over the density of states of the occupation probability of a given state. For a nucleus with mass A in an internal state with spin J, the density of states is

$$(2J + 1)\, \mathrm{d}^3k_A/(2\pi)^3 \,. \tag{7.23}$$

The occupation probability of a given state $\boldsymbol{k}_A$ is

$$\exp[-(\hbar^2k_A^2/2mA - E_\beta - \mu_A)/T] \tag{7.24}$$

where E_β is the binding energy of the nucleus in the state J, μ_A is the chemical potential of this species, and T is the temperature. The density of these nuclei is then

$$\begin{aligned}\rho_A &= [4\pi(2J + 1)/(2\pi)^3] \int k^2\, \mathrm{d}k \exp(-\hbar^2k^2/2mAT) \exp[(E_\beta - \mu_A)/T] \\ &= (1/2\pi^2)(2J + 1)(2mAT/\hbar^2)^{3/2}(\tfrac{1}{2}\pi^{1/2}\cdot\tfrac{1}{2}) \exp[(E_\beta - \mu_A)/T] \,.\end{aligned} \tag{7.25}$$

If there is equilibrium between all species, the sum of the chemical potentials of the products of any possible reactions must equal the sum of the initial chemical potentials. Thus, if the nucleus A has N protons and Z neutrons, the chemical potentials must satisfy

$$\mu_A = N\mu_\mathrm{n} + Z\mu_\mathrm{p} \tag{7.26}$$

where μ_n and μ_p are the chemical potentials of neutrons and protons. These are related to the density of neutrons or protons by

$$\rho_{\mathrm{n,p}} = 2(mT/2\pi\hbar^2)^{3/2} \exp(-\mu_{\mathrm{n,p}}/T) \,. \tag{7.27}$$

Using eqs. (7.25) and (7.27), we can express the density of species A in terms of the proton and neutron densities,

$$\rho_A = (2J + 1)\left(\frac{mAT}{2\pi\hbar^2}\right)^{3/2} \exp(E_\beta/T)\, \frac{1}{2^A} \left(\frac{2\pi\hbar^2}{mT}\right)^{(3/2)A} \rho_\mathrm{n}^N \rho_\mathrm{p}^Z \,. \tag{7.28}$$

This formula has an important application in astrophysics, the determination of the abundances of elements formed in the beginning of the universe, when it was small and extremely hot [7.10]. From the present characteristics of the universe, one can infer the relation between size and temperature of the universe as it expands. Nuclear reactions will cease at some point when the temperature is too low to allow Coulomb barriers to be penetrated, which is about 100 keV. The density at this point works out to be such that helium is the second most abundant species, after hydrogen.

To apply eq. (7.28) to nuclear collisions, we need to know the density and temperature at which the system freezes into its final distribution of species. If the initial energy of the collision is distributed over A nucleons, and we assume that this mass expands adiabatically, the temperature is related to the density by

$$TV^{\gamma-1} = \text{const.} \,, \qquad \rho/\rho_0 = (T/\tfrac{2}{3}E)^{3/2} \,, \tag{7.29}$$

where E is the initial energy per particle. We next have to determine independently the density at which the relative abundances are fixed. This requires information on the cross-sections for production and break-up of nuclei. In terms of these cross-sections, the rate at which transformations take place is

$$\sigma v_\mathrm{rel}\rho \,,$$

where v_rel is the relative velocity of the interacting species. The adiabatic expansion hypothesis, eq. (7.29), implies that

$$v_\mathrm{rel} \simeq (R_0/R)v_0 \,,$$

where R is the radius of the expanding system at a given time, and v_0 is the initial relative velocity. The time t_f at which a given species will have made its last collision is given by

$$\int_{t_\mathrm{F}}^{\infty} \mathrm{d}t\sigma v_\mathrm{rel}\rho = 1 \,.$$

Converting the time integral to an integral over R,

$$\mathrm{d}t = \mathrm{d}R/v\,,$$

and expressing ρ in terms of R, we find that this condition is equivalent to

$$\frac{1}{3}\frac{\sigma}{v}v_0\frac{\rho_0 R_0^4}{R^3} = 1 \qquad \text{or} \qquad \rho_\mathrm{f} = \rho_0\frac{R_0^3}{R^3} = \frac{3v}{\sigma v_0 R_0}\,. \tag{7.30}$$

In the range of temperatures and densities of interest, $T \sim 10$ MeV and $\rho \lesssim \rho_0$, eq. (7.28) predicts that the most abundant species is the nucleons, followed by deuterons. A typical cross-section for $\mathrm{d} + \mathrm{p} \to \mathrm{p} + \mathrm{p} + \mathrm{n}$ is 100 mb. Substituting this cross-section in eq. (7.30), together with $R_0 \approx 5$ fm, the freeze-out density works out to

$$\rho_\mathrm{f} \simeq 0.06\ \mathrm{fm}^{-3}\,,$$

roughly half of nuclear matter density. Substituting this into eq. (7.28) and assuming $T = 50$ MeV, we find that the ratio of deuterons to protons is

$$\rho_\mathrm{d}/\rho_\mathrm{p} = \tfrac{3}{4}2^{3/2}(2\pi\hbar^2/mT)^{3/2}\rho_\mathrm{n}\exp(2/T) \simeq 0.75\,. \tag{7.31}$$

At the temperatures we are considering, the exponential factor in eq. (7.31) does not play a significant role in this estimate: it is basically just the density of deuteron-like states that is important. The idea of simply looking at density of states has been used in an ad hoc manner to extract the abundances of deuterons and other light fragments [7.11].

The heavier fragments emerging at low energies remain a problem for theory. These fragments emerge nearly isotropically in collisions at 2.1 GeV/A (ref. [7.12]). Their energy distribution more or less requires a temperature of ~ 5 MeV/nucleon. At lower energies, 400 and 500 MeV/A, the angular distribution is distinctly not isotropic, but is forward peaked. The data can be roughly fit if it is assumed that the target emits the particles isotropically while travelling at a velocity of 0.06–0.08c (see ref. [7.13] also). The first question we should ask is why angular distribution should become more isotropic at higher energy. Perhaps this could be understood in a two-fluid model: at higher energy, the energy deposited in the target approaches in magnitude the momentum deposited, according to eq. (7.20). Thus, for a given energy deposited in the target, there will be more momentum at lower bombarding energies. If this is the explanation, there should be a saturation effect: going to even higher energies will not change the ratio of momentum to energy, so the 2.1 GeV/A results should persist at even higher projectile energies.

References

[1.1] J. R. Adam et al., J. Applied Physics 39 (1968) 5173.
[1.2] G. R. Satchler, Phys. Letters 55B (1975) 167.
[1.3] J. R. Birkelund et al., Phys. Rev. C13 (1976) 128.
[1.4] J. R. Huizenga et al., Phys. Rev. Letters 37 (1976) 885.
[1.5] H. Gauvin et al., Nucl. Phys. A223 (1974) 103.
[1.6] J. B. Natowitz et al., Phys. Rev. C6 (1972) 2133.
[1.7] H. H. Gutbrod et al., Phys. Rev. C14 (1976) 1808.
[1.8] R. Albrecht et al., Phys. Rev. Letters 34 (1975) 1400.
[1.9] P. Glässel et al., Phys. Rev. Letters 38 (1977) 331.
[1.10] K. Van Bibber, et al., Phys. Rev. Letters 38 (1977) 334.
[1.11] F. Pougheon, Orsay preprint.
[1.12] P. Dyer et al., Phys. Rev. Letters 39 (1977) 392.
[1.13] H. Heckman et al., Atlas of Heavy Ion Topology, unpublished.
[1.14] D. E. Greiner et al., Phys. Rev. Letters 35 (1975) 152.
[1.15] C. Gelbke et al., Phys. Letters 65B (1976) 227.
[1.16] H. Gutbrod et al., Phys. Rev. Letters 37 (1976) 667.
[1.17] G. D. Westfall et al., Phys. Rev. Letters 37 (1976) 1202.
[1.18] B. Jakobsson et al., Nucl. Phys. A276 (1977) 253.
[1.19] J. Stevenson et al., Phys. Rev. Letters 38 (1977) 1125.
[1.20] J. Papp et al., Phys. Rev. Letters 34 (1975) 601.
[1.21] H. Andrä et al., Phys. Rev. Letters 37 (1976) 1212.
[1.22] A. Galonsky, private communication.
[1.23] P. McNulty et al., Phys. Rev. Letters 38 (1977) 1519.
[2.1] N. Bogoliubov and K. Gurov, J. Exp. Theo. Phys. (USSR) 17 (1947) 614.
[2.2] N. Bogoliubov, J. Phys. (USSR) 10 (1946) 256;
M. Born and H. Green, A General Kinetic Theory of Liquids (Cambridge, 1949);
J. G. Kirkwood, J. Chem. Phys. 15 (1947) 72;
J. Yvon, La Théorie Statistique des Fluides (Hermann, 1935).
[2.3] E. Wigner, Phys. Rev. 40 (1932) 749.
[2.4] Suggested by P. Carruthers.
[2.5] J. Negele and D. Vautherin, Phys. Rev. C5 (1972) 1472.
[2.6] A. Vlasov, J. Phys. (USSR) 9 (1945) 25.
[2.7] E. Madelung, Z. Phys. 40 (1926) 322.
[2.8] E. Gross, J. Math. Phys. 4 (1964) 195.
[2.9] L. Landau, J. Phys. (USSR) 10 (1946) 25.
[2.10] L. Landau, Soviet Phys. JETP 3, (1956) 920.
[2.11] T. Deal and S. Fallieros, Phys. Rev. C7, (1973) 1709.
[2.12] J. Noble, Ann. Phys. (New York) 67 (1971) 98.
[3.1] J. Martorell et al., Phys. Letters 60B (1976) 313.
[4.1] K. Huang and C. N. Yang, Phys. Rev. 105 (1957) 767.
[4.2] C. DeDominicis and P. Martin, Phys. Rev. 105 (1957) 1417.
[4.3] W. Myers and W. Swiatecki, Ann. Phys. 55 (1969) 395.
[4.4] D. Vautherin and D. Brink, Phys. Rev. C5 (1972) 626.
[4.5] L. Zamick, Phys. Letters 45B (1973) 313.
[4.6] S. Chin and J. Walecka, Phys. Letters 52B (1974) 24.

[4.7] J. Błocki et al., Ann. Phys. (N.Y.) 105 (1977) 427.
[5.1] V. M. Galitskii, Sov. Phys. JETP 7 (1958) 104.
[5.2] K. Kikuchi and M. Kawai, Nuclear Matter and Nuclear Reactions, (North-Holland, 1968).
[5.3] N. Metropolis et al., Phys. Rev. 110 (1958) 204.
[5.4] V. Barashenkov and V. Maltsev, Fortschritte der Physik 9 (1961) 553.
[5.5] "NN and ND Interactions" Lawrence Radiation Lab, UCRL 20,000, (1973).
[5.6] J. Jeukenne et al., Physics Reports 25C (1976) 83.
[5.7] A. Bohr and B. Mottelson, Nuclear Structure Vol. I (Benjamin, 1969), p. 165.
[5.8] C. Perez and F. Perez, Atomic Data 17 (1976) 2.
[5.9] P. Morel and P. Nozières, Phys. Rev. 126 (1962) 1909.
[5.10] A. Abrikosov and I. Khalatnikov, Rept. Progr. Phys. 22 (1959) 329.
[6.1] D. A. Tidman and N. A. Krall, Shock Waves in Collisionless Plasmas, (Wiley–Interscience, 1971).
[6.2] P. Bonche et al., Phys. Rev. C13 (1976) 1226.
[6.3] C. Y. Wong et al., Phys. Letters 66B (1977) 19.
[6.4] V. Ruck et al., Z. Phys. A277 (1976) 391.
[6.5] R. Sawyer, Nucl. Phys. A271 (1976) 235.
[6.6] R. Cusson et al., Phys. Rev. Letters 36 (1976) 1166.
[6.7] J. Nix, Nucl. Phys. A130 (1969) 241.
[6.8] K. Davies et al., Phys. Rev. C13 (1976) 2385.
[6.9] W. Scheid et al., Phys. Rev. Lett. 32 (1974) 741.
[6.10] M. Sobel et al., Nucl. Phys. A251 (1975) 502.
[7.1] J. Papp et al., Phys. Rev. Letters 34 (1975) 601.
[7.2] G. Fujioka et al., J. Phys. Soc. Japan 39 (1975) 1131.
[7.3] K. Gottfried, Phys. Rev. Letters 32 (1974) 957.
[7.4] O. Bernay et al., NN and ND Interactions, (Lawrence Rad. Lab., 1970).
[7.5] L. Landau and E. Lifshitz, Fluid Mechanics (Pergamon, 1959) 355.
[7.6] A. Amsden et al., Phys. Rev. Letters 35 (1975) 905.
[7.7] A. Amsden, A. Goldhaber, F. Harlow and J. Nix, Phys. Rev. C17 (1978) 2080.
[7.8] A. Amsden et al., Phys. Rev. Letters 38 (1977) 1055.
[7.9] A. Mekjian, Phys. Rev. Letters 38 (1977) 640.
[7.10] E. Burbridge et al., Rev. Mod. Phys. 29 (1957) 547.
[7.11] H. Gutbrod et al., Phys. Rev. Letters 37 (1976) 667.
[7.12] B. Jakobsson et al., Nucl. Phys. A276 (1977) 253.
[7.13] J. Stevenson et al., Phys. Rev. Letters 38 (1977) 1125.
[7.14] J. Hüfner and J. Knoll, Nucl. Phys. A290 (1977) 460.

SEMINAR 2

CHARACTERISTIC TIME SCALES IN DEEP INELASTIC HEAVY ION COLLISIONS*

John W. HARRIS

Department of Physics,
State University of New York at Stony Brook,
Stony Brook, New York 11794, USA

Contents

* Supported in part by the US National Science Foundation.

R. Balian et al., eds.
Les Houches, Session XXX, 1977. Ions lourds et mésons en physique nucléaire/Nuclear physics with heavy ions and mesons